



universität  
wien

# DIPLOMARBEIT / DIPLOMA THESIS

Titel der Diplomarbeit / Title of the Diploma Thesis

“Printable Formulations For Macroporous Polymers Useful  
For Battery Applications”

verfasst von / submitted by

Hoai Maria Nguyen Thu BSc

angestrebter akademischer Grad / in partial fulfilment of the requirements for the degree of  
Diplom-Ingenieurin (Dipl.-Ing./ DI)

Wien, 2018/ Vienna, 2018

Studienkennzahl lt. Studienblatt /  
degree programme code as it appears on  
the student record sheet:

A 066 658

Studienrichtung lt. Studienblatt /  
degree programme as it appears on  
the student record sheet:

Masterstudium Chemie und Technologie der  
Materialien UG2002

Betreut von / Supervisor:

Univ.-Prof. Dipl.-Chem. Dr. Alexander Bismarck



## Abstract

Separators are decisive in all batteries, as they keep the anode and cathode apart to avoid electrical short circuits, meanwhile allowing ionic charge carriers to pass. State of the art separator's manufacturing is time consuming, as it is done in a multistep process, hence quite energy consuming. PolyHIPEs address the need of a highly porous material and the possibility of doing a one pot synthesis of in situ electrolyte filled battery separators, merely using the electrolyte as internal phase. Furthermore, a broad spectrum of electrolytes can be used from pH one to 14. Fabrication of polyHIPEs via emulsion templating make it possible to print the separator straight on the electrode before polymerisation, which contribute to a swift process. As separators limit the performances of electrolytes, our results indicate low performance limitations for all investigated systems, possessing MacMullin numbers of two to three.



I wish to express my sincere thanks to Professor Alexander Bismarck for giving me the opportunity to work in his group PaCE (Polymer and Composite Engineering). I am extremely thankful and indebted to him for his support.

I would like to express my sincere gratitude to my co-supervisor Werner Paschinger, MSc for his support and patience. He always had an open door to answer my questions. He has allowed me to work independently, but he always steered me in the right direction whenever he thought I needed it. I could not have imagined having a better advisor.

Finally, I would like to thank my parents Hang and Hung, my sister Jenny and my godmother Margit Steiner for their unceasing encouragement and support throughout my years of study. I am also grateful to my partner Philipp Wolschner, who always supported me. This accomplishment would not have been possible without them. Thank you very much.

---

---

## Table of Content

<b>1.</b>	<b>INTRODUCTION</b> .....	<b>1</b>
<b>1.1.</b>	<b>State of the art separators for nickel-metal hydride batteries</b> .....	<b>1</b>
<b>1.2.</b>	<b>State of the art polyethylene pocket separators for lead acid batteries</b> .....	<b>2</b>
<b>1.3.</b>	<b>High internal phase emulsions (HIPEs) for separator applications in lithium ion batteries</b> .....	<b>3</b>
<b>2.</b>	<b>EXPERIMENTAL PART</b> .....	<b>5</b>
<b>2.1.</b>	<b>Materials</b> .....	<b>5</b>
2.1.1.	For the synthesis of separators for NiMH batteries .....	5
2.1.2.	For the synthesis of separators for lead-acid batteries .....	5
2.1.3.	For the synthesis of separators for lithium ion batteries .....	6
<b>2.2.</b>	<b>Preparation of polymerised high internal phase emulsions (polyHIPEs)</b> .....	<b>6</b>
2.2.1.	Preparation of aqueous polymerised high internal phase emulsions (polyHIPEs) .....	6
2.2.2.	Preparation of non-aqueous polymerised high internal phase emulsions (polyHIPEs) .....	7
<b>2.3.</b>	<b>Characterisation of polymerised high internal phase emulsions (polyHIPEs)</b> .....	<b>8</b>
2.3.1.	Measurement of pore- and pore throat sizes.....	8
2.3.2.	Measurement of porosities .....	9
2.3.3.	Specific surface area measurement.....	9
2.3.4.	Ionic conductivity of polymerised high internal phase emulsions (polyHIPEs) .....	10
2.3.5.	Thermal stability of polymerised high internal phase emulsions (polyHIPEs).....	11
2.3.6.	Thermal transitions polymerised high internal phase emulsions (polyHIPEs).....	12
<b>2.4.</b>	<b>Battery testing of different battery systems</b> .....	<b>12</b>
2.4.1.	Battery testing of nickel-metal hydride (NiMH) batteries .....	12
2.4.2.	Battery Testing of lead acid batteries .....	12
2.4.3.	Battery Testing of lithium ion batteries.....	13
<b>3.</b>	<b>RESULTS AND DISCUSSION</b> .....	<b>13</b>
<b>3.1.</b>	<b>Results and discussion on aqueous polymerised high internal phase emulsions (polyHIPEs)</b> .....	<b>13</b>
3.1.1.	Results and discussion on polymerised high internal phase emulsions (polyHIPEs) with KOH as internal phase .....	13
3.1.1.	Results and discussion on polymerised high internal phase emulsions (polyHIPEs) with H <sub>2</sub> SO <sub>4</sub> as internal phase .....	24

---

---

3.1.	Results and discussion on non-aqueous polymerised high internal phase emulsions (polyHIPEs) ....	30
4.	CONCLUSION.....	38
5.	REFERENCES.....	IV

---

## 1. Introduction

Separators play a substantial key role in batteries<sup>1,2</sup>. A separator is a porous non-conductive material, which is located between a negative and a positive electrode to isolate them from each other and prevent short circuits. Simultaneously, they must allow the passage of ionic charge carriers and thereby minimise as much as possible the additional resistance caused by the separator matrix to permit maximum ionic conductivity of the electrolyte. Separators with many open pores (high porosity) with the least possible diameter are desired, to inhibit the migration of particles. For instance, in lead acid batteries, where the migration of liberated lead particles, could result in a short circuit, if they pass the separator. The separator should be wetted by the electrolyte quickly, since time-consuming steps would go along with high production costs. Being chemically inert in an acidic or alkaline environment for lead acid or nickel-metal hydride (NiMH) batteries is mandatory. Furthermore, high resistance in the presence of strong oxidizing and reducing conditions is expected. Another important separator requirement is the thermal stability. Separators must withstand heat generation during charge and discharge processes of the cells.

Shirshova *et al.*<sup>3</sup> introduced the use of high internal phase emulsions, abbreviated polyHIPEs (chapter 1.3), filled with ionic liquids as separators for lithium ion batteries. In their previous work<sup>4</sup>, they examined the immiscibility of different monomers with an ionic liquid and concluded, that lauryl methacrylate (LMA) was suitable. There is no separator which can be used in all battery systems. This thesis should prove, whether it is possible to extend their method to the synthesis of aqueous HIPEs for applications in NiMH and lead acid batteries. Kot *et al.*<sup>5</sup> investigated different bis(trifluoromethane)sulfonimide lithium salt (LiTFSI) concentrations in a mixture of 50:50 ethylene carbonate (EC) and propylene carbonate (PC). This concept was adapted for highly concentrated electrolytes<sup>6</sup>. These electrolytes consisted of different lithium salts, which were dissolved in a mixture of EC and PC for lithium batteries.

### 1.1. State of the art separators for nickel-metal hydride batteries

Nickel-metal hydride batteries are an advancement of sealed Ni-Cd batteries. They are in generally perceived as being more environmentally-friendly, due to the fact, that the negative cadmium-based electrode is replaced by a metal alloy electrode soaked with hydrogen-gas. Compared to NiCd systems, NiMH batteries exhibit higher energy densities, due to their lower separator thickness of 120  $\mu\text{m}$  - 210  $\mu\text{m}$ <sup>7</sup>. Thinner separators can be implemented, as the

---

electrolyte is not absorbed during charging, and therefore, the separator does not function as electrolyte consumer or contributor.<sup>8</sup>

Less research is done in the field of separators used in secondary alkaline systems compared to separators in lithium batteries or lead acid batteries<sup>1,2</sup>. However, it is well known, that the biggest drawback of NiMH batteries - the high rate self-discharge behaviour - can be reduced by the separator<sup>9,10,11,12,7,13,14,15</sup>. Besides, NiMH systems are used in many commercially available hybrid electric vehicles, although they are increasingly displaced by Li-ion batteries.

The German company Freudenberg is the leading supplier of separators for NiMH batteries in the world and the only producer outside of China<sup>16</sup>. However, Freudenberg applied only for 8 patents between 1993 and 2010<sup>16</sup>, much more active research is done in China. In comparison, 14 Chinese patents were filed between 2009 and 2016<sup>17</sup>.

Separators used in NiMH batteries must be chemically inert in the presence of high concentrated aqueous KOH-based electrolytes. Most commonly the NiMH-electrolyte contains 20-36% KOH solution<sup>18</sup> and is chosen because of its high ionic conductivity<sup>19</sup>. Furthermore, the separator needs to stay saturated with the electrolyte solution the entire time. Predominantly polyolefine nonwovens are used due to their high porosity<sup>8</sup>. Nonwovens are materials in which many layers of disordered fibres - in this case made of synthetic polymers as polyolefines – are stapled. The fabrication of nonwoven separators is done in three steps: generation of the web, attachment of the fibres to each other and as final step post-treatment<sup>8</sup>. Nonwovens reach porosities between 50-75% with maximum pore sizes of around 15  $\mu\text{m}$ <sup>8</sup> for NiMH battery systems.

## 1.2. State of the art polyethylene pocket separators for lead acid batteries

Pocket type PE separator are used in passenger cars. Commonly, porosities are around 60%, to not sacrifice mechanical stability of the separator matrix<sup>20</sup>. The average pore size is 0.1  $\mu\text{m}$ <sup>21</sup>. Such reduction in average pore size – compared to other lead acid separators<sup>21</sup> – is necessary due to the fact, that lead particles have diameters of around 1 to 5  $\mu\text{m}$  and their passage would come along with deposition of shed particles in the pores which could trigger a short circuit<sup>21</sup>. The PE separator has a thickness of around 0.25  $\mu\text{m}$ <sup>21</sup>. The separator has to be stable over a temperature range from -40°C to 100°C<sup>20</sup>. The manufacturing process is shown in detail in the “Handbook of Battery Materials” and is divided into three steps<sup>22</sup>.

### 1.3. High internal phase emulsions (HIPEs) for separator applications in lithium ion batteries

Emulsions are created from two immiscible liquids. Most commonly an aqueous solution phase and an organic- or oil phase.<sup>23</sup> After Lissant's categorisation<sup>24</sup>, emulsions, which comprise an internal phase or dispersed phase volume of more than 70%, are called HIPEs. However, Cameron *et al.*<sup>23</sup> suggest, a "more precise definition would be [...] [that] those with an internal phase volume above 74.05%"<sup>23</sup>, are classed as HIPEs. They reasoned their statement with the fact, that - after Lissant's already mentioned work - at 0.74 the internal phase volume reaches the upmost accessible occupation of regular formed, non-distorted spherical droplets. Above this volume fraction - until 0.94 - they possess a polyhedral shape and will take the shape of a rhomboidal dodecahedral (RDH).

HIPEs are generated under steady stirring of the external, or continuous phase with the subsequent added primary internal phase. The internal phase is dispersed within an external phase. Due to the coalescence and/ or Ostwald ripening during polymerisation, the structure of the initial HIPE and the polymerised (polyHIPE) can be different from one another. By polymerizing the continuous phase of a HIPE, polyHIPEs are created. Pores and interconnects are created at the flimsiest sites of the continuous phase which creates an open porous structure. The external phase encloses the internal phase and will provide the skeleton of the polyHIPE. The distinct droplets of the HIPEs dispersed phase assume a polyhedral packing. Consequently, junctions occur and continuous interconnected polyHIPEs are obtained.<sup>25</sup> Synthesis of polymers within the HIPE is possible, if a monomer is part of the continuous phase – as described above-, the dispersed phase or both phases.

Using polyHIPEs as separators in lithium ion batteries were proposed by Shirshova *et al.*<sup>3</sup> and Kot *et al.*<sup>5</sup>. The formulations used by them included the monomer lauryl methacrylate (LMA), the crosslinker 1,14-tetradecane-diol dimethacrylate (TDDMA), the surfactant CITHROL DPHS-SO-(MV) and the initiator 2, 2' Azobis(isobutyronitrile) (AIBN) in their external phase. Only the internal phase, which comprised the electrolyte solution was different: bis(trifluoromethane)sulfonimide lithium salt (LiTFSI) in 1-ethyl-3-methylimidazolium bis(trifluoromethylsulfonyl)imide (IL)<sup>3</sup> or bis(trifluoromethane)sulfonimide lithium salt (LiTFSI) in a blend of EC (ethylene carbonate) and PC (propylene carbonate)<sup>5</sup>. Production of the separator was done in one single step and the separator scaffold was already filled with

---

electrolyte. Shirshova *et al.*<sup>3</sup> noted, that there is a dependency of lithium salt concentration and the average pore diameter and average pore throat size. According to them, there appears to be two possible reasons for this behaviour. An increasing lithium salt concentration results in a higher viscosity of the dispersed phase, which is accompanied by separation of droplets and the creation of greater droplets. It could also be that, that the miscibility of external in the internal phase rises with increasing lithium salt concentrations, leading to a reduced HIPE stability. Moreover, the crosslinker to monomer ratio was varied and they ascertained a rise in ionic conductivity by using a surplus of monomer. In their set of data no correlation between conductivity and average pore size or average pore throat size was found. By adjusting the internal phase, the porosity was tuned. However, the lithium salt concentration was still too low, to be used in commercial lithium ion batteries, therefore Kot *et al.*<sup>5</sup> aimed to increase the concentration between 0.5 to 1.5 M. They changed the electrolyte, since with 1-ethyl-3-methylimidazolium bis(trifluoromethylsulfonyl)imide (IL) the maximum concentration of LITFSI was only 0.06 M.

Xu<sup>26</sup> listed demands, how an exemplary electrolyte solvent should perform. An electrolyte should maintain its liquid state over a wide temperature range. They should not chemically react with parts of the battery cell. Furthermore, a high dielectric constant is considered desirable, consequently it is accompanied by the ability to dissolve numerous different lithium salts. To achieve high voltage, particularly active electrodes are used, which undergo severe redox reactions. For this reason, solvents containing active protons are excluded and, therefore, no aqueous electrolytes are used, although they have beneficial properties, such as high conductivity and good salt solvation. Suitable electrolyte solvents are non-aqueous containing nitrile, an ether bridge, sulfonyl or a carbonyl as polar group. Propylene carbonate meet these requirements, but concerning its behaviour to decompose (Xu<sup>26</sup> and Zhao *et al.*<sup>27</sup> summarized discussions of issues concerning PC degradation in their work) and exfoliation in the presence of graphite electrodes<sup>6</sup>, an electrolyte as co-solvent is needed. Ethylene carbonate has advantageous properties<sup>28</sup> with regard to its high dielectric constant and low viscosity - which simplifies ion transport – makes it an excellent solvent. But due to its melting point of 36.2°C<sup>28</sup>, ethylene carbonate is solid at RT and its application as sole electrolyte would be in conjunction with restrictions in respect of possible temperature ranges deployed in the battery cell. The melting point of EC can be lowered, by adding only 9% PC<sup>29</sup>, so a liquid solution at RT can be gained. EC as co-solvent<sup>30,31,32,33,5</sup> is preferred because of its ability of to

---

form passivation films<sup>31</sup>, unlike PC. After coating the graphite electrode with this film no further degradation of the electrolyte was observed. This film was named - after Peled's<sup>34</sup> work from 1979 - SEI (solid electrolyte interphase). A review on SEI formation was provided by Xu<sup>26</sup>.

Current reviews concerning the progress of investigating highly concentrated electrolytes for lithium batteries is given by Yamada *et al.*<sup>6</sup> and Zheng *et al.*<sup>35</sup>. Increasing the lithium salt concentration over 1 M was usually accompanied by an increased viscosity and a decreased ionic conductivity, which are both undesirable. Therefore, not much attention was paid to this class of electrolytes. Ogumi and co-worker<sup>36,37</sup> revived the public interest. They stated, that lithium intercalation into the graphite electrode depends on the electrolyte concentration. Dissolving 2.72 M lithium bis(perfluoroethylsulfonyl)imide (LiBETI)<sup>36</sup> in pure PC did not lead to delamination of graphite, as generally observed when using a solution of 1 M concentrated lithium salt dissolved in PC. Instead a reversible charge-discharge of the battery cell was observed, without decomposition of the electrolyte. The aroused interest in these highly concentrated electrolytes can be confirmed by two review articles<sup>6,35</sup>, within two years.

## 2. Experimental part

### 2.1. Materials

#### 2.1.1. For the synthesis of separators for NiMH batteries

All chemicals were used as received: The surfactant CITHROL DPHS-SO-(MV) (kindly provided by Croda Europe Ltd), lauryl methacrylate (LMA) (96%, Sigma Aldrich), 1,12 dodecanediol dimethacrylate (DDDMA) (95%, abcr GmbH) and Darocur<sup>®</sup> 1173 (kindly provided by BASF) were used. Potassiumhydroxide (KOH) pellets (technical grade, ACM Chemicals) were dissolved in deionized water to obtain a 20 wt% KOH solution.

#### 2.1.2. For the synthesis of separators for lead-acid batteries

Span<sup>®</sup> 80 (Fluka Analytical), lauryl methacrylate (LMA) (96%, Sigma Aldrich), 1,12 dodecanediol dimethacrylate (DDDMA) (95%, abcr GmbH), Irgacure 819 (kindly provided by BASF) and sulfuric acid solution (5M, Titripur<sup>®</sup>) (Sigma Aldrich) were used as supplied.

### 2.1.3. For the synthesis of separators for lithium ion batteries

The following chemicals were employed without preliminary purification steps. HYPERMER 1083 (kindly provided by CRODA Europe Ltd), lauryl methacrylate (LMA) (96%, Sigma Aldrich), 1,12 dodecanediol dimethacrylate (DDDMA) (95%, abcr GmbH),  $\alpha$ ,  $\alpha'$  azoisobutyronitrile (AIBN) (98%, Sigma Aldrich). Different lithium salts were explored: lithium tetrafluoroborate ( $\text{LiBF}_4$ ) (anhydrous, powder, 99.99% trace metals basis, Sigma Aldrich), lithium hexafluorophosphate ( $\text{LiPF}_6$ ) (battery grade,  $\geq 99.99\%$  trace metals basis, Sigma Aldrich), lithium perchlorate ( $\text{LiClO}_4$ ) (battery grade, dry,  $\geq 99.99\%$  trace metals basis, Sigma Aldrich), lithium bis(trifluoromethane)sulfonimide ( $\text{LiTFSI}$ ) ( $\text{LiN}(\text{SO}_2\text{CF}_3)_2$ ) (99.95% trace metals basis, Sigma Aldrich), lithium hexafluoroarsenate ( $\text{LiAsF}_6$ ) (95%, Sigma Aldrich), lithium difluoro(oxalate)borate ( $\text{LiDFOB}$ ) ( $\text{LiBF}_2(\text{C}_2\text{O}_2)$ ) (Sigma Aldrich). As solvent for the lithium salts a blend of ethylene carbonate (EC) (anhydrous, 99%, Sigma Aldrich) and propylene carbonate (PC) (anhydrous, 99.7%, Sigma Aldrich) was used.

## 2.2. Preparation of polymerised high internal phase emulsions (polyHIPEs)

### 2.2.1. Preparation of aqueous polymerised high internal phase emulsions (polyHIPEs)

The polyHIPE film formation was inspired by Shirshova *et al.*<sup>4,3</sup> and Kot *et al.*<sup>5</sup> Aqueous HIPEs were produced in a glass reaction vessel endowed with a glass paddle rod, which was coupled to an overhead stirrer. Dissolving the surfactant (7.5, 15 and 25 wt% with respect to the monomer mixture) in a mixture of LMA with the crosslinker DDDMA and the initiator, resulted in the continuous phase. The molar ratio of the monomer and crosslinker were equal. Under continuous agitation at a rate of 400 rpm, the internal phase - the electrolyte - was added dropwise to the external phase. Finally, the stirring rate was increased to 2000 rpm for 1 min. Through the higher energy input, a greater shear rate ensured the homogenisation of the emulsion, which resulted in smaller sized droplets. The emulsion was transferred onto a glass substrate and casted using a casting machine (K Printing Proofer, RK Print Coat Instruments) and polymerised by exposure to UV light (UV lamp; DYMAX UVC-8 Light-Curing Conveyor, DYMAX®):  $880 \text{ mW/cm}^2$ ,  $1 \text{ m min}^{-1}$ , for three runs in open air. The samples were named after the percentage of dispersed phase and the surfactant used (*Table 1*).

Table 1 Sample composition of aqueous polyHIPEs used KOH as internal phase (abbreviated K) and H<sub>2</sub>SO<sub>4</sub> as internal phase (abbreviated S). Used materials for the preparation of aqueous polyHIPEs are listed in chapter 2.1.1 for KOH as dispersed phase and 2.1.2 for H<sub>2</sub>SO<sub>4</sub> as dispersed phase.

Sample	Continuous phase				Dispersed phase		
	Monomer:Cross -linker	Surfactant		Initiator		KOH	H <sub>2</sub> SO <sub>4</sub>
		CITHROL	Span® 80	Darocur® 1173	Irgacure 819		
		[%]	[%]	[%]	[%]	[%]	[%]
K75_7.5	1:1	7.5	-	10	-	75	-
K75_15	1:1	15	-	10	-	75	-
K75_25	1:1	25	-	10	-	75	-
K80_7.5	1:1	7.5	-	10	-	80	-
K80_15	1:1	15	-	10	-	80	-
K80_25	1:1	25	-	10	-	80	-
K85_7.5	1:1	7.5	-	10	-	85	-
K85_15	1:1	15	-	10	-	85	-
K85_25	1:1	25	-	10	-	85	-
K90_7.5	1:1	7.5	-	10	-	90	-
K90_15	1:1	15	-	10	-	90	-
K90_25	1:1	25	-	10	-	90	-
K95_7.5	1:1	7.5	-	-	-	95	-
K95_15	1:1	15	-	10	-	95	-
K95_25	1:1	25	-	-	-	95	-
S75_7.5	1:1	-	7.5	-	-	-	75
S75_15	1:1	-	15	-	5	-	75
S75_25	1:1	-	25	-	10	-	75
S80_7.5	1:1	-	7.5	-	-	-	80
S80_15	1:1	-	15	-	1	-	80
S80_25	1:1	-	25	-	4	-	80
S85_7.5	1:1	-	7.5	-	-	-	85
S85_15	1:1	-	15	-	1	-	85
S85_25	1:1	-	25	-	2	-	85
S90_7.5	1:1	-	7.5	-	-	-	90
S90_15	1:1	-	15	-	3	-	90
S90_25	1:1	-	25	-	3	-	90
S95_7.5	1:1	-	7.5	-	-	-	95
S95_15	1:1	-	15	-	-	-	95
S95_25	1:1	-	25	-	-	-	95

### 2.2.2. Preparation of non-aqueous polymerised high internal phase emulsions (polyHIPEs)

As a first step, ratios of EC and PC were altered by dissolving 1 M LiClO<sub>4</sub> and HIPEs were formed. Due to the high ionic conductivity of PC, the highest possible amount of PC was pursued. Yet, HIPEs containing a higher amount of PC than EC were not stable or did not form polyHIPEs after polymerization. Thus, it was decided to continue the work with a 50:50 mixture of EC/PC. The next step involved the discovery of the highest possible amount of LiClO<sub>4</sub>, while still being able to form a stable HIPE. Formation of HIPEs with internal phases

---

containing a maximum of 3.9 M LiClO<sub>4</sub> dissolved in 50:50 EC/PC was observed. Experiments mentioned until now, were all carried out in air. However, the other salts (chapter 2.1.3) contain fluoride in their structure, which could lead to the release of HF. Therefore, the experiments were performed in a glovebox (UNIlab Pro Glove Box, MBRAUN). In argon atmosphere stable HIPEs with even 4.9 M LiClO<sub>4</sub> were realised. In the presence of air a concentration of only 3.9 M was possible. The 4.9 M concentrated lithium salts were dissolved under steady stirring in 50:50 EC/PC. Lithium salts, which dissolved under these superconcentrated conditions were: LiBF<sub>4</sub>, LiClO<sub>4</sub>, LiAsF<sub>6</sub>, LiPF<sub>6</sub> and LiTFSI.

Since the conductivity of an electrolyte depends very much on the temperature, the resistivity was measured within the temperature range of 15 – 100°C. The temperature was increased in steps of 5°C. The lithium electrolyte with the maximum ionic conductivity over a broad temperature range was picked for emulsion templating in argon atmosphere. HIPE were prepared in a glass reaction vessel. The surfactant and initiator (following the chosen amount for K85\_15 in *Table 1*) were dissolved in a blend of 2:1 monomer LMA and DDDMA. The electrolyte was added drop wise under permanent stirring at a rate of 400 rpm. Finally, the agitation speed was increased to 2000 rpm for 1 min to produce homogeneous emulsions.

Casting, which was executed in a glovebox, took place on a glass substrate with the (K Printing Proofer, RK Print Coat Instruments). For polymerization a hand UV lamp (100 W, 365 nm, 50 Hz, 2.0 A, Black Ray, B-100 AP HIGH Intensity, UVP, Cambridge, UK) was set up in the glovebox.

### 2.3. Characterisation of polymerised high internal phase emulsions (polyHIPEs)

Ionic conductivity was measured before extraction and drying. All the remaining characterisation methods were performed after extraction of the internal phase. For purification, the polyHIPE films were rinsed out with distilled water (for aqueous HIPEs) or acetone (for non-aqueous HIPEs). The wash solutions were altered several times. For the samples with a water-based internal phase, the washing was continued until a pH of 7 was reached. Subsequently, the samples were dried in an oven at 50°C overnight.

#### 2.3.1. Measurement of pore- and pore throat sizes

Scanning electron microscopy (SEM) (JCM-6000 Benchtop SEM – JEOL) was used to investigate the separator morphology. An accelerating voltage of 15 kV was applied. Samples were sputter coated with gold (JFC-1200 Fine Coater – JEOL) for 30 s in an argon environment and imaged using a JCM-6000 Benchtop SEM (JEOL) with an electron beam voltage of 15 kV.

---

---

Images at 2200 x magnification were analysed using the measurement tool in ImageJ. 100 randomly chosen pores and pore throats were considered for determination of the average pore throat and pore size.

### 2.3.2. Measurement of porosities

Porosity was determined by the ratio of void density (envelope density  $\rho_E$ ) to matrix density (skeletal density  $\rho_S$ ) (1):

$$\varepsilon[\%] = \left(1 - \frac{\rho_E}{\rho_S}\right) \times 100\% \quad (1)$$

To determine the skeletal density, the measured volume excludes pores. It is a non-destructive method, since the technique uses inert gas (He) as displacement medium to determine the absolute volume. 1g of a polyHIPE sample was triturated by a mortar. The results were obtained by using the gas pycnometer AccuPyc II 1340 from Micromeritics Instrument Corporation.

An envelope density analyser (GeoPyc 1360, Micromeritics Instrument Corporation) was utilized to determine the envelope density. The envelope density includes pore spaces in the volume measurement. The sample was placed into a bed of a dry solid medium called Dry Flo. This medium ensures close packing without penetrating in the pores owing to its rigid and small spheres, hence it possess a high flow-ability. A precision cylinder was filled with dry medium and a plunger compacts the whole content to get a zero-volume baseline. In a second run, the sample was added to the cylinder. The different heights how much the plunger penetrates the cylinder were used to determine the displacement volume and thereby the sample volume. Sample weight divided by sample volume is the envelope density  $\rho_E$ .

3 random pieces of a sample were weighed and the porosity  $\varepsilon$  was calculated via (1 by GeoPyc 1360.

### 2.3.3. Specific surface area measurement

Characterisation of the specific surface area, which is defined as the total surface area of a material per unit of mass, is impaired by adsorbed contaminants on the surface. Removal was done by cutting up the sample into small pieces and putting these batches in a degassing station of the FlowPrep™ 060. A stream of inert gas He and heat of 120°C were applied to the

sample overnight. The TriStar II Surface Area and Porosity Micromeritics, which uses the Brunauer-Emmett-Teller model (BET) to calculate the specific surface area, was employed to determine the capillary condensation and physical adsorption of N<sub>2</sub>. The nitrogen adsorption was measured under isothermal conditions.

#### 2.3.4. Ionic conductivity of polymerised high internal phase emulsions (polyHIPEs)

Determination of the separator resistance was done by planting the with electrolyte filled separator between two electrodes. AC impedance method is applied to measure the resistance  $R$  at a certain frequency. At the chosen frequency, the separator impedance is equal to the electrolyte resistance or separator resistance. Various (at least 6 per sample) measurements were executed to get low measurement inaccuracy. Equation (2):

$$\rho = \frac{R \cdot A}{l} \quad (2)$$

describes the relationship between the specific resistivity  $\rho$ , the measured resistance  $R$ , the conductor's cross-section  $A$  and length  $l$ . Unless otherwise stated, the resistance  $R$  was measured at 25°C.

The ionic conductivity  $\sigma$  is defined as the reciprocal value of the specific resistivity  $\rho$ .

$$\sigma = \frac{1}{\rho} \quad (3)$$

Measurements of the ionic conductivity of KOH were realised in a TSC 1600 measuring cell (Metrohm AG) and for separators containing KOH as internal phase experiments were carried out in a closed TSC SW (Metrohm AG) measurement cell. Cells were connected to a GAMRY Reference 600 potentiostat. For polyHIPEs containing H<sub>2</sub>SO<sub>4</sub> as internal phase, a homemade equipment, consisting of two massive copper blocks as electrodes connected to a GAMRY Reference 600 potentiostat were established, to measure the resistance  $R$ . Measurements were performed at room temperature. The ionic conductivity measurements for all lithium electrolytes were carried out using a closed TSC 1600 (Metrohm AG) liquid sample cell. A two-electrode setup was chosen with polished platinum working and counter electrodes. The

sample cell was filled with about 1.0 ml electrolyte and thermostated with an accuracy of  $\pm 0.1$  K by a Eurotherm 2416 temperature controller.

The performance of the electrolyte is restricted by the separator matrix. The MacMullin number<sup>38</sup>  $N_M$  is a decisive parameter to describe the separator performance. The number is expressed as a ratio of the electrical resistance ( $\rho_{sep}$ ) of the electrolyte soaked sample and the resistance of the electrolyte ( $\rho_{el}$ ) (4). Alternatively, it can be determined via the relationship between conductivity of the pure electrolyte ( $\sigma_{el}$ ) and conductivity of the porous media saturated with the electrolyte ( $\sigma_{sep}$ ).

$$N_M = \frac{\rho_{sep}}{\rho_{el}} = \frac{\sigma_{el}}{\sigma_{sep}} \quad (4)$$

MacMullin  $N_M$  number can be related to the tortuosity  $\tau$ <sup>39</sup>:

$$N_M = \frac{\tau}{\varepsilon} = \frac{R_{ION} \cdot A \cdot \sigma_{el}}{d} \quad (5)$$

The parameters are ionic resistance  $R_{ION}$ , cross-section area  $A$  of the separator, ionic conductivity  $\sigma_{el}$ , thickness  $d$  of the separator sample. Other ways of defining the tortuosity exist<sup>39</sup>, however this approach (equation (5)) was chosen as method of choice, due to the accessibility of the tortuosity value through experiments.

### 2.3.5. Thermal stability of polymerised high internal phase emulsions (polyHIPEs)

In commercial microporous membranes, separators start to decompose at about 135°C<sup>1</sup>. When using water-based electrolytes, it is necessary to ensure that degradation of the separator matrix does not occur at the electrolyte's boiling point, to prevent a short circuiting and a possible explosion of the battery. The thermal stability was characterised by thermogravimetric analysis (TGA) (Discovery TGA – TA Instruments). The amount of weight change of a sample was measured as a function of temperature. Samples were heated from 30 to 500°C at a heating rate of 10°C min<sup>-1</sup> in nitrogen atmosphere. Small sample pieces with a weight of 10-20 mg were investigated.

### 2.3.6. Thermal transitions polymerised high internal phase emulsions (polyHIPEs)

To study thermal transitions in polyHIPE samples during heating it, differential scanning calorimetry (Discovery DSC – TA Instruments) was used. It investigates, how temperature changes the heat capacity of a material. The samples were pestled and placed into an aluminium zero pan with hermetic zero lid. An empty pan was utilized as reference. Measurements were performed three times under nitrogen atmosphere in the temperature range from -80 to 120 °C and a heating rate of 10°C min<sup>-1</sup> was used.

## 2.4. Battery testing of different battery systems

### 2.4.1. Battery testing of nickel-metal hydride (NiMH) batteries

A NiMH-battery cell was built up using the PAT-Cell assembly (EL-CELL). A nickel alloy was used as negative electrode and Ni(OH)<sub>2</sub> as positive electrode (both kindly provided by VARTA) were separated by the polyHIPE separator containing 20 wt% KOH. The cell was mounted into an EL-CELL PAT-Stand-16 connected to a BaSyTec battery test system for CC-CV (constant current-constant voltage) cycling between 1.0 V and 1.42V at room temperature.

The long-running stability of a battery was characterized by repeating charge and discharge cycles. The capacity *C* describes the energy stored by a battery. The capacity *C* is measured in ampere-hours (Ah), which describes how many hours a battery can maintain the same current to the discharge rate at the nominal voltage of the battery. The coulombic efficiency  $\eta_c$  was calculated:

$$\eta_c = \frac{C_{discharge}}{C_{charge}} \quad (6)$$

$C_{charge}$  and  $C_{discharge}$  represent the charge ratio during charging and discharging.

### 2.4.2. Battery Testing of lead acid batteries

A lead acid battery (5×5 cm) was built by attaching a separator between two lead foils (0.1 mm in thickness, Sigma Sigma Aldrich). The whole attachment was sealed between two pieces of Plexiglas. The battery was connected to a GAMRY Interface 5000P Galvanostat and galvanostatic cycling was performed between 1.75V and 2.85V. Current density was set to 50 μA·cm<sup>-2</sup> for charging and 25 μA·cm<sup>-2</sup> for discharging.

### 2.4.3. Battery Testing of lithium ion batteries

A cell was assembled composing of  $\text{Li}[\text{Li}_{1/3}\text{Ti}_{5/3}]\text{O}_4$  (LTO) on aluminum foil as anode and  $\text{Li}(\text{Ni}_{1/3}\text{Mn}_{1/3}\text{Co}_{1/3})\text{O}_2$  (NMC) on aluminum foil as cathode (both kindly provided by Fraunhofer IZM). All components were build up in a TSC Battery Cell (rhd instruments). The cell was connected to a GAMRY Reference 600 Potentiostat and CC-CV cycling was performed between 1.8 V and 2.85 V at a C/10 rate. The C-rate describes how fast the charging and discharging takes place. C/10 means, that over a period of 10 hours the battery has been completely discharged. The loading of the electrodes were  $2 \text{ mAh}\cdot\text{cm}^{-2}$  respectively. Temperature was kept constant at  $25 \text{ }^\circ\text{C}$  ( $\pm 0.1 \text{ }^\circ\text{C}$ ) using a Eurotherm 2416 temperature controller.

## 3. Results and discussion

### 3.1. Results and discussion on aqueous polymerised high internal phase emulsions (polyHIPEs)

#### 3.1.1. Results and discussion on polymerised high internal phase emulsions (polyHIPEs) with KOH as internal phase

A series of HIPEs was generated using an aqueous dispersed phase and an external phase consisting of varying amounts of surfactant and monomer (*Table 1*). Use of crosslinking comonomers, targeted the avoidance of polyHIPE collapse during polymerisation and drying<sup>40</sup>. Immiscibility of the dispersed and external phase is essential to obtain a stabile HIPE. As the internal phase is aqueous, a hydrophobic continuous phase is desirable. This precondition is given by utilizing a crosslinker with a hydrophobic backbone, which exhibits a high similarity in structure with the monomer LMA. Due to the unavailability of TDDMA (1,14-tetradecanediol dimethacrylate)<sup>4,3,5</sup>, the experiments were carried out using DDDMA (1,12-Dodecanedioldimethacrylate).

Referring to Shirshova et al.<sup>4,3</sup> chosen surfactant concentrations, polyHIPEs with 7.5, 15 and 25 wt.% surfactant were synthesised. The polyHIPE morphologies were studied by using SEM (*Figure 1*). For K75\_25 (*Figure 1c*) and K80\_25 (*Figure 1f*) a strut-like structure was obtained. A polyHIPE containing 80 vol% internal phase and 25 wt.% surfactant with a bicontinuous structure is corroborated by literature<sup>4,3,5</sup>. For 75 vol% KOH no literature was found. Williams et al.<sup>41</sup>, Shirshova et al.<sup>4,3</sup> and Kot et al.<sup>5</sup> found, that an increase in surfactant concentration

---

correlates with changes in polyHIPE structure. After passing the ideal surfactant concentration, they recognized changes in the structure. No interconnectivity was observed anymore, rather the creation of struts, or bicontinuous structures. It was possible to create a typical HIPE structure when using 25 wt.% surfactant in the formulation, when the dispersed ratio contained 85 vol% (*Figure 1i*) and 90 vol% (*Figure 1l*). The typical pore structure could be found for K85\_25 and K90\_25. The existence of an ideal amount of surfactant for HIPE formation cannot be confirmed from the available data. The internal phase does not seem to exert influence on the structure of the polyHIPE films<sup>41</sup> alone and the parameters responsible for the formation of a classical HIPE structure are much more complex. For instance, HIPEs with 75 vol% and 80 vol% dispersed phase and a 7.5 wt.% (*Figure 1a, Figure 1d*) and 15 wt.% surfactant amount (*Figure 1b, Figure 1e*) exhibit a porous scaffold with interconnects. Concerning the high porosity in K95\_15 (*Figure 1m*), the pores and pore throats are of the same size. Shrinkage after drying was observed for this sample, indicating a low stability of the polyHIPE due to the low crosslinker amount, which comes along with loss in mechanical stability and collapse during drying<sup>40</sup>. For K95\_7.5 (*Figure 1j*) and K95\_25 (*Figure 1l*) phase separation occurred and the formation of a HIPE was not possible.

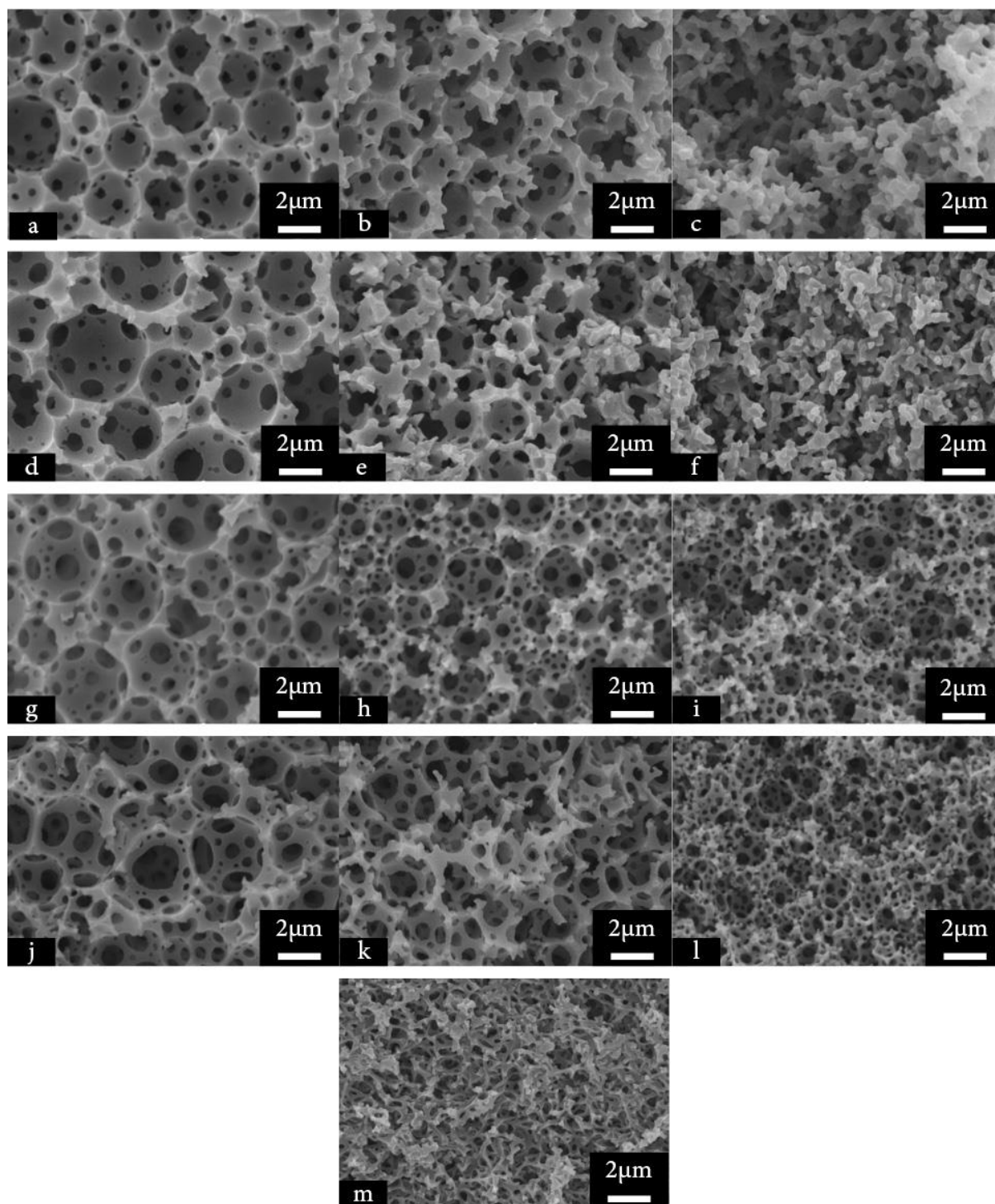


Figure 1 SEM images of polyHIPE films: (a) K75\_7.5, (b) K75\_15, (c) K75\_25, (d) K80\_7.5, (e) K80\_15, (f) K80\_25, (g) K85\_7.5, (h) K85\_15, (i) K85\_25, (j) K90\_7.5, (k) K90\_15, (l) K90\_25, (m) K95\_15. For composition see *Table 1*.

Determination of the average pore size  $D$  was performed using the image analysis software Image J. Each set of calculation contained 100 pores. As the pores are not perfectly spherical, for each pore the lowest diameter and the biggest lengths were considered, to calculate the mean of the pore throat diameter  $d$ . Samples with 25 wt.% surfactant, which did not develop

well-defined pores were excluded from analysis. K85\_25 (Figure 1i) and K90\_25 (Figure 1l) present cavity diameters of around 1  $\mu\text{m}$ , which is one magnitude smaller in comparison to the other samples with a typical polyHIPE structure (Table 2). Average pore throat sizes were defined with the same method as for the average pore diameter. Repeatedly, the two named samples with 25 wt.% of surfactant were smaller and no more than half the size of the other samples, which had interconnected pore throats (Table 2).

Table 2 Properties of polyHIPEs prepared with KOH as internal phase: specific surface area, average pore diameter  $\langle D \rangle$ , average pore throat diameter  $\langle d \rangle$ , skeletal density, porosity, onset temperature  $T_0$

Sample	Specific surface			Skeletal density $\rho_s$	Porosity $\epsilon$	$T_0$ (TGA)
	area (BET)	$\langle D \rangle$ (SEM)	$\langle d \rangle$ (SEM)			
	$[\text{m}^2 \text{g}^{-1}]$	$[\mu\text{m}]$	$[\mu\text{m}]$	$[\text{g cm}^{-3}]$	$[\%]$	$[\text{°C}]$
K75_7.5	5.77	2.17 $\pm$ 0.77	0.38 $\pm$ 0.14	1.058	78	206
K75_15	5.24	1.92 $\pm$ 0.57	0.45 $\pm$ 0.18	1.043	78	215
K75_25	6.63	-	-	1.045	77	219
K80_7.5	5.65	2.49 $\pm$ 1.14	0.45 $\pm$ 0.21	1.057	83	208
K80_15	6.78	1.87 $\pm$ 0.75	0.42 $\pm$ 0.17	1.053	83	226
K80_25	7.12	-	-	1.057	80	226
K85_7.5	8.53	2.41 $\pm$ 0.98	0.37 $\pm$ 0.21	1.057	87	228
K85_15	8.88	1.13 $\pm$ 0.6	0.3 $\pm$ 0.18	1.041	87	233
K85_25	14.08	0.98 $\pm$ 0.41	0.19 $\pm$ 0.12	1.048	86	246
K90_7.5	12.58	1.9 $\pm$ 1.08	0.36 $\pm$ 0.26	1.069	92	260
K90_15	11.06	1.91 $\pm$ 0.97	0.34 $\pm$ 0.22	1.049	91	275
K90_25	23.68	0.99 $\pm$ 0.38	0.18 $\pm$ 0.11	1.038	90	278
K95_15	-	-	-	1.049	94	248

A higher surfactant concentration resulted in a decrease in pore diameter (Table 2). With increasing surfactant amount the emulsion stability increased and smaller droplet sizes were stabilised in the HIPE. Thus, the smaller pore sizes in the polyHIPE. Because of the lower interfacial tension, a greater interfacial area is allowed<sup>42</sup>. This is particularly well visible for the samples K85\_25 and K90\_25, where the increase in pore and pore throat diameter was the largest and a major increase in specific surface area occurred. With increasing internal phase, the specific surface area enlarges too. Cameron<sup>42</sup> suggests, that the film, which occurs at the interface between aqueous internal phase and the hydrophobic mixture of surfactant and monomer, gets more pronounced due to the fact, that the hydrophilic phase vol. ratio increases. This interfacial film limits or even inhibits Ostwald ripening. Therefore, smaller HIPE droplets can remain and smaller pore diameters can be formed. Due to smaller droplet sizes,

---

the interfacial tension is lowered and a larger interfacial area can exist, hence a greater specific surface area. The skeletal densities were around  $1 \text{ g cm}^{-3}$ , which is consistent with literature<sup>4</sup>. For samples which possessed cavities, the determined porosities correlated with the amount of internal phase used in the template (*Table 2*). This proves the influence of dispersed phase ratios on gaining tailored porosities. While commercial nonwoven separators reach porosities up to 75%<sup>8</sup>, it can be tuned for polyHIPE separators by controlling the emulsion phase vol. ratio.

Overheating of batteries leads to degradation and evaporation of electrolyte fluids, which is followed by gasification, which causes flame formation. 20% KOH is dissolved in the aqueous phase. Thus, the boiling point is slightly above  $100^\circ\text{C}$ . Thermal stability of the separator scaffold is essential. The separator should be thermally stable under these conditions. All TGA curves exposed resembling temperature profiles, showing the same trend of decomposition. The extrapolated onset temperature  $T_0$  marks the temperature at which the weight loss sets in (*Figure 2*).  $T_0$  of the polyHIPE scaffolds are similar with the values found in Shirshova et al.<sup>4</sup> work. The thermal degradation commences at approximately  $200^\circ\text{C}$  and delays the onset by further addition of dispersed phase and surfactant. Due to the higher amount of surfactant, the polyHIPE is better stabilised, leading to the delayed onset.

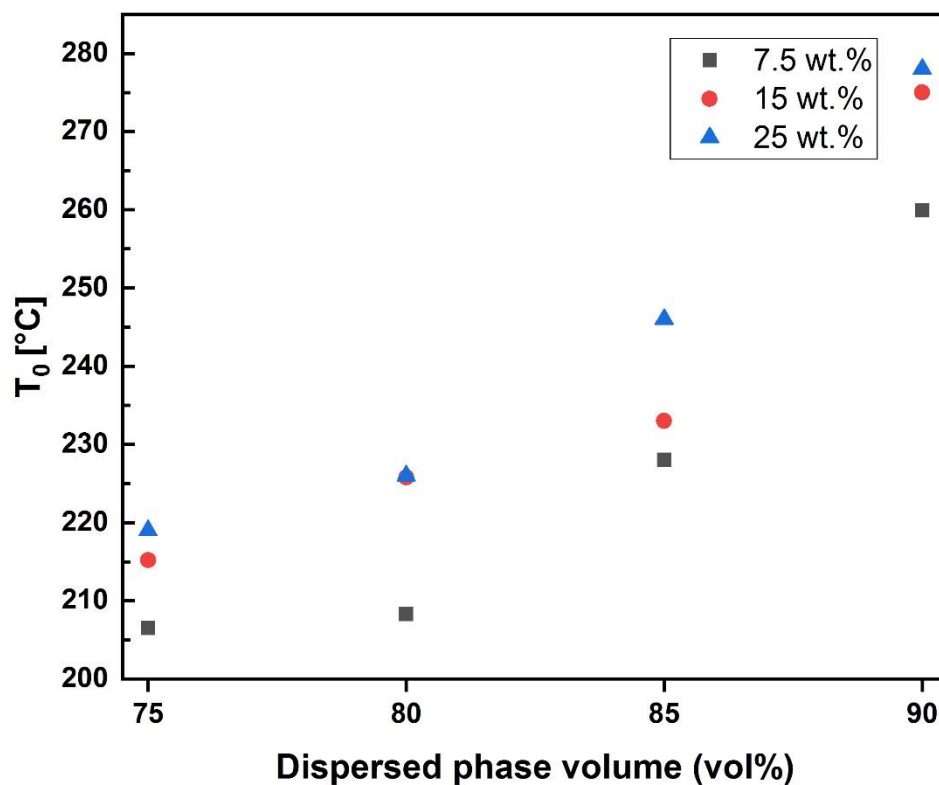


Figure 2 Dependence between extrapolated onset temperature  $T_0$ , internal phase ratio and surfactant content (7.5 wt.%, 15 wt.%, 25 wt.%)

To determine the thermal behaviour, the DSC thermograms were evaluated. Samples were extracted from their internal phase before measurement. The DSC curves for samples with an extracted dispersed phase of 75 vol% (Figure 3) are representative for the other measured samples not shown here. Two small endothermic peaks at  $-10^{\circ}\text{C}$  and  $-1^{\circ}\text{C}$  can be seen, representing the melting of the surfactant, as they become more pronounced with increasing surfactant concentration. More importantly, crosslinked polymers cannot melt due to their high cross-linking level and would degrade after exceeding their decomposition temperature.

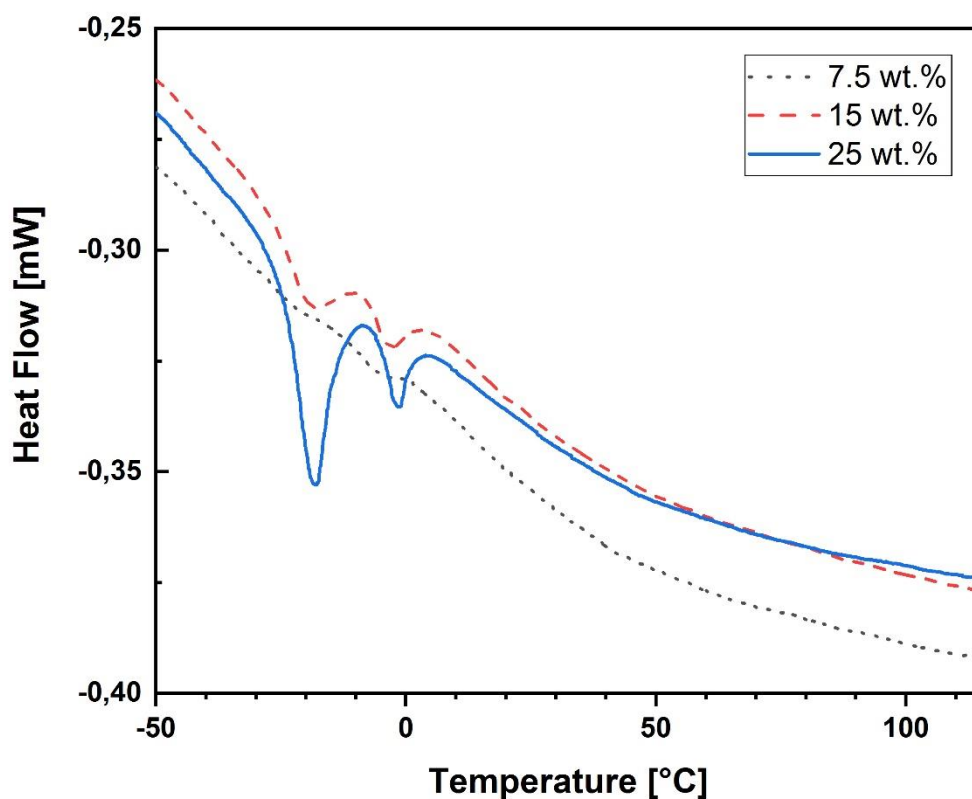


Figure 3 Representative DSC thermograms from the second run for the scaffolds with 75 vol% of internal phase and their respective surfactant ratio (7.5 wt. %, 15 wt.%, 25 wt.%)

For polyHIPE compositions of 80 vol% potassiumhydroxide (KOH) the ionic conductivity for 15 wt.% surfactant was  $28.2 \text{ mS cm}^{-1}$  and alters to  $30.7 \text{ mS cm}^{-1}$  for 7.5 wt.% surfactant (Figure 4). Prior work<sup>3,5</sup> has documented that ionic conductivity increases with increasing surfactant amount for LMA based polyHIPEs. Their investigated systems contained a dispersed volume of around 80 vol% 0.06 M solution of LITFSI in 1-ethyl-3-methylimidazolium bis(trifluoromethylsulfonyl)imide (IL). They decreased the surfactant amount from 15 wt.% to 7.5 wt.% and the ionic conductivity changed from  $8.6 \text{ mS cm}^{-1}$  to  $7.5 \text{ mS cm}^{-1}$ . However, they only investigated polyHIPE systems with an internal phase of 80 vol%. Figure 4 shows ionic conductivity measurements of samples with internal phases between 75 vol% and 95 vol%. The received data do not support the theory of a dependency between surfactant concentration and ionic conductivity. This position is supported by the ionic conductivities of Kot *et al.*<sup>5</sup>. Their samples had an internal phase of 83 vol%, which consisted of 0.06M LITFSI in

EC/PC 50:50 wt.%. They discovered a slight decline of ionic conductivity from  $1.44 \text{ mS cm}^{-1}$  (15wt.% of surfactant) to  $1.10 \text{ mS cm}^{-1}$  (25 wt.% of surfactant).

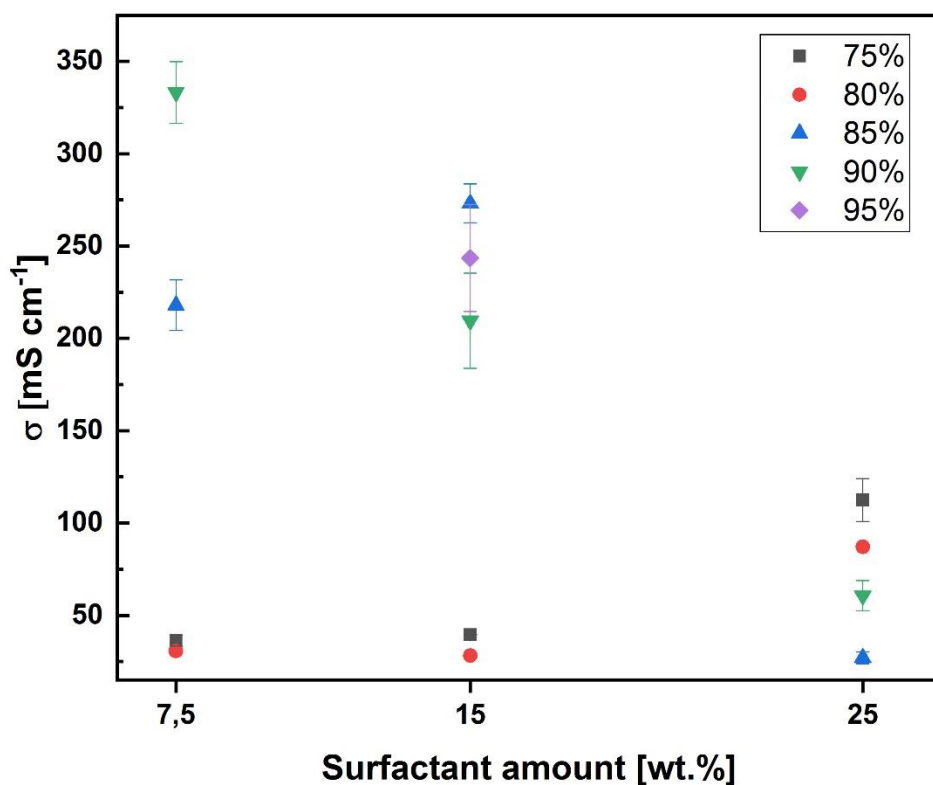


Figure 4 Relationship between surfactant ratio and conductivity measured at 25°C

Converting the standard deviations of the experimentally exceeded ionic conductivities (*Figure 4*) from  $\text{mS cm}^{-1}$  in percentage, the deviations were only between 3-4%, which suggests a good reproducibility of the measurements. Standard deviations reported in the literature<sup>3</sup> for LMA based continuous phases with an internal phase of ionic liquid-in-oil of 80 vol% are higher. For K75\_25 and K80\_25 the inhomogeneous strut-like structure made it impossible to predict a consistent ionic conductivity over the whole separator area and therefore, it is not suitable for battery applications. In addition, the polyHIPEs, which had this bicontinuous structures were fragile regarding mechanical stability<sup>5</sup>. As mentioned above, the porosities can be tuned by the phase vol. ratio of the emulsion template. For higher amounts of internal phase, which is the electrolyte KOH, higher porosities are achieved, and thus, higher ionic conductivities are expected. However, the data (*Figure 4*) indicate, that a greater average in pore- or pore throat size does not automatically correlate with an increased ionic conductivity. When utilizing a

---

surfactant concentration of 7.5 wt.%, the highest ionic conductivity was obtained with 90 vol% KOH electrolyte. This evidence cannot be transferred to the surfactant amounts of 15 wt.% and 25 wt.%. It can be assumed, that ionic conductivity is influenced by more parameters than the porosity. From the available data, high ionic conductivities do not depend merely on specific surface area, pore size or surfactant concentration (*Table 2*). It is clear, that much additional work is required before a complete understanding of how ionic conductivity is influenced, can be reached. To understand the deprivations in conductivity loss in the separator matrix in terms of electrolyte conductivity, the Mac Mullin number was used. A MacMullin number of 1 implies that the separator scaffold does not affect the bulk electrolyte conductivity. Arora *et al.*<sup>43</sup> used a 40% potassium hydroxide electrolyte solution. Their separators had porosities of around 50% and 77% and MacMullin numbers between 4 to 6. Samples used in this thesis, contain an electrolyte concentration of 20% KOH. Even MacMullin numbers of around one were achieved indicating that the separator scaffold hardly affected the ionic conductivity (*Table 3*). Proceeding from the microstructure, one would expect lower MacMullin number for sample K90\_25 (*Figure 1i*) than K90\_7.5 (*Figure 1j*). This indicates, that relationships between microstructure and conductivity are much more complex. Furthermore, determination of the MacMullin number provides an insight into the microstructure of the material, because of the closely linked relationship to porosity and tortuosity (chapter 2.3.4). The tortuosity is around one for K90\_7.5 (*Table 3*), which suggests that the separator should not affect ion transport.

Table 3 Porosity, MacMullin Number: measured ionic conductivity for KOH was  $484.42 \text{ mS cm}^{-1}$ , tortuosity

Sample	$\epsilon$ Porosity [-]	$N_M$ MacMullin Number [-]	$\tau$ Tortuosity [-]
K75_7.5	0.78	13.5±1.1	10.5±0.8
K75_15	0.78	12.3±0.1	9.6±0.1
K75_25	0.77	4.4±0.4	3.3±0.3
K80_7.5	0.83	15.8±0.7	13.1±0.6
K80_15	0.83	17.2±0.5	14.3±0.4
K80_25	0.80	5.6±0.1	4.4±0.1
K85_7.5	0.87	2.2±0.1	1.9±0.1
K85_15	0.87	1.8±0.1	1.5±0.1
K85_25	0.86	18.2±2.1	15.6±1.8
K90_7.5	0.92	1.5±0.1	1.3±0.1
K90_15	0.91	2.3±0.3	2.1±0.3
K90_25	0.90	8.1±1.0	7.3±0.9
K95_15	0.94	2±0.2	1.9±0.2

Figure 5 shows the first charge (black) and discharge (red) curve. Voltage (continuous lines) and current (dashed lines) are plotted over time. During battery charging, the voltage increases constantly. Potentiostatically, the cell is held at 1.32 V until the current approaches 2.6 mA, which guarantees the full charge of the battery. At the start of the discharge stage, the voltage drops. A low drop of the voltage is desired, to get out the highest possible output energy of the battery. At 1 V, the discharge ended and the battery is fully discharged. A discharge of around 4 hours meets the discharge time of conventional Panasonic<sup>44</sup> NiMH batteries.

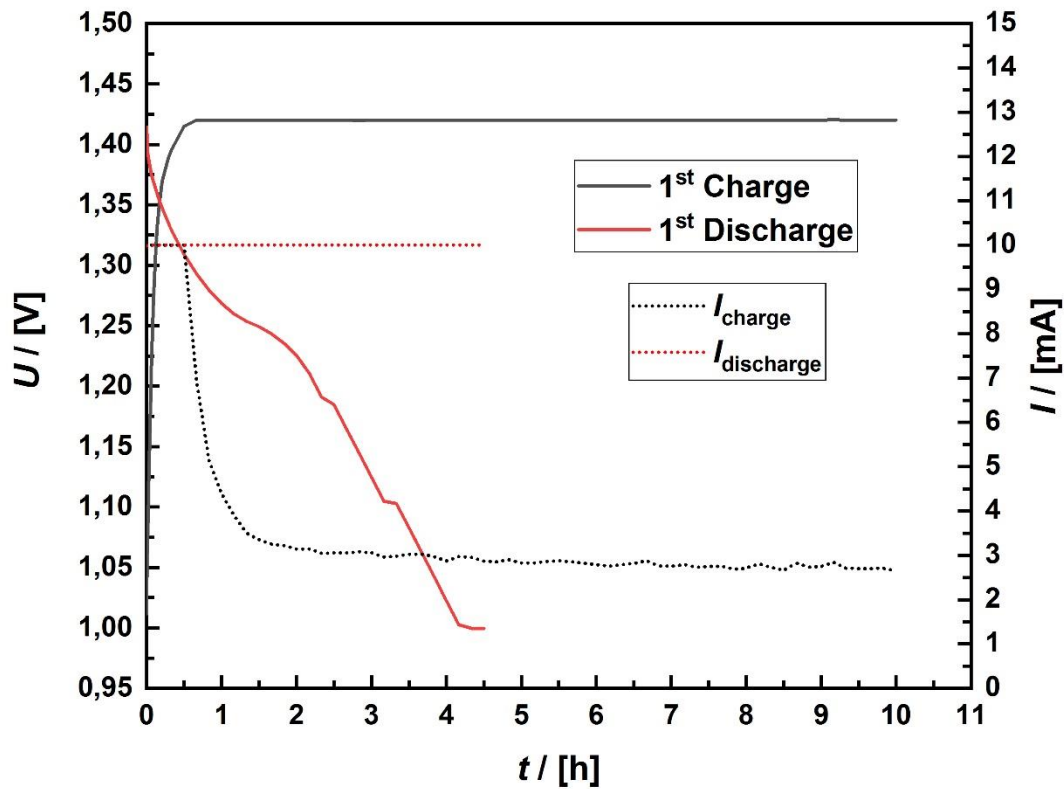


Figure 5 Charge and discharge curve of a NiMH battery (first cycle)

The charge capacity at first cycle has a value of 35 mAh: It increased rapidly to 47 mAh after the 3<sup>rd</sup> cycle (Figure 6). In the first few cycles, the lower charge capacities can be associated with stabilisation of the system. After the 21<sup>st</sup> cycle it reaches its maximum at 60 mAh and the cell maintains its electrochemical stability. For the first cycle the discharge capacity is 26 mAh. At 55 mAh at the 24<sup>th</sup> cycle the cell is stable. The values of coulombic efficiency are depicted in (Figure 6). The efficiency increases slightly from 0.75 in the first cycle to 0.91 in the 21<sup>st</sup> cycle and remains there after 32 cycles. However, testing a battery through cycling is a long-term experiment. Currently the battery is still running, therefore only 32 cycles are shown.

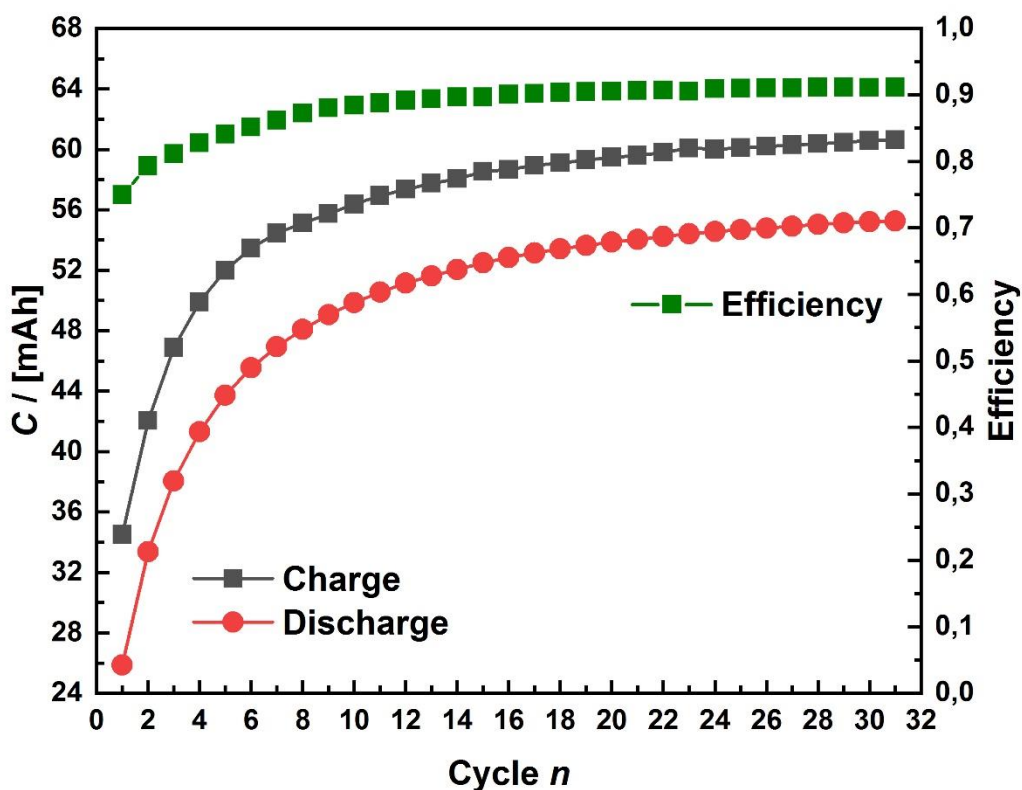


Figure 6 Charging and discharging over 31 cycles (NiMH system)

### 3.1.1. Results and discussion on polymerised high internal phase emulsions (polyHIPEs) with $\text{H}_2\text{SO}_4$ as internal phase

Figure 7 depicts all polyHIPE compositions which did not undergo phase-separation and formed stable polyHIPEs. In their morphologies they reflect the earlier described KOH-filled counterparts. However, S75\_15 (Figure 7a) does not seem to have well defined pore walls as the other samples with  $\text{H}_2\text{SO}_4$  as internal phase. Furthermore, before polymerisation S75\_15 acted almost fluid like. For the unpolymerised sample S90\_25 (Figure 7f) printing was difficult because of its high viscous texture.

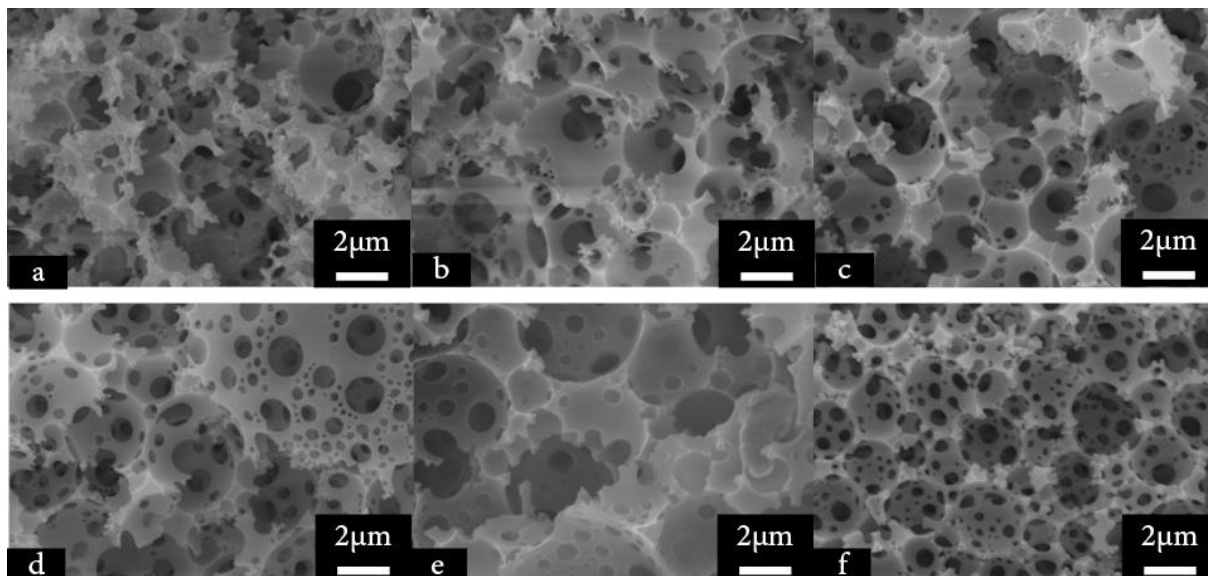


Figure 7 SEM images of polyHIPE films: (a) S75\_15, (b) S80\_15, (c) S85\_15, (d) S85\_25, (e) S90\_15, (f) S90\_25. For sample composition see *Table 1*.

The average pore size and pore throat diameters were measured (chapter 2.3.1). The highest average pore diameters of around 2  $\mu\text{m}$  were obtained, when using a surfactant concentration of 15 wt.% and a dispersed phase volume of 80% or 90%. Before polymerisation these two samples (*Figure 7a*, *Figure 7f*), caused problems due to their texture, which made it difficult to print an even separator without pinholes. They have the smallest average pore sizes and average pore throat diameters. Yet, the standard deviations of  $\langle D \rangle$  (*Table 4*) are in the same size range, indicating a more inhomogeneous structure for the samples containing sulfuric acid with respect to the samples entailing potassium hydroxide (*Table 2*).

An increase of specific surface area (*Table 4*) was observed, when adding further amounts of dispersed phase and increasing the surfactant amount. Reasons for this data progress are found in chapter 3.1.1. The results for the skeletal densities (*Table 4*) are consistent with the results found for the films containing CITHROL DPHS-SO-(MV) in their scaffold (*Table 2*). The porosities can be tuned by altering the internal phase vol. ratio the samples containing  $\text{H}_2\text{SO}_4$  as electrolyte (*Table 4*).

Table 4 Properties of polyHIPeS prepared with  $H_2SO_4$  as internal phase: specific surface area, average pore diameter  $\langle D \rangle$ , average pore throat diameter  $\langle d \rangle$ , skeletal density, porosity, onset temperature  $T_0$

Sample	Specific surface area (BET) [ $m^2 g^{-1}$ ]	$\langle D \rangle$ (SEM) [ $\mu m$ ]	$\langle d \rangle$ (SEM) [ $\mu m$ ]	Skeletal density $\rho_s$ [ $g cm^{-3}$ ]	Porosity $\epsilon$ [%]	$T_0$ (TGA) [ $^{\circ}C$ ]
S75_15	3.26	1.21±0.64	0.27±0.19	1.154	75	269
S80_15	4.66	1.72±0.96	0.33±0.23	1.125	82	230
S85_15	7.05	1.96±1.54	0.41±0.26	1.132	87	236
S85_25	7.57	1.69±1.49	0.37±0.3	1.146	87	224
S90_15	7.45	2.10±1.32	0.47±0.34	1.175	90	243
S90_25	10.56	1.43±0.87	0.23±0.18	1.127	90	284

All extrapolated onset temperatures  $T_0$  range between 224  $^{\circ}C$  and 284 $^{\circ}C$  (Figure 8) and therefore, they are far away from the boiling point of the aqueous electrolyte. However, a correlation between the surfactant concentration, the internal phase ratio and  $T_0$  cannot be found like for the potassium hydroxide samples, because in this case we used another surfactant (chapter 2.1.2).

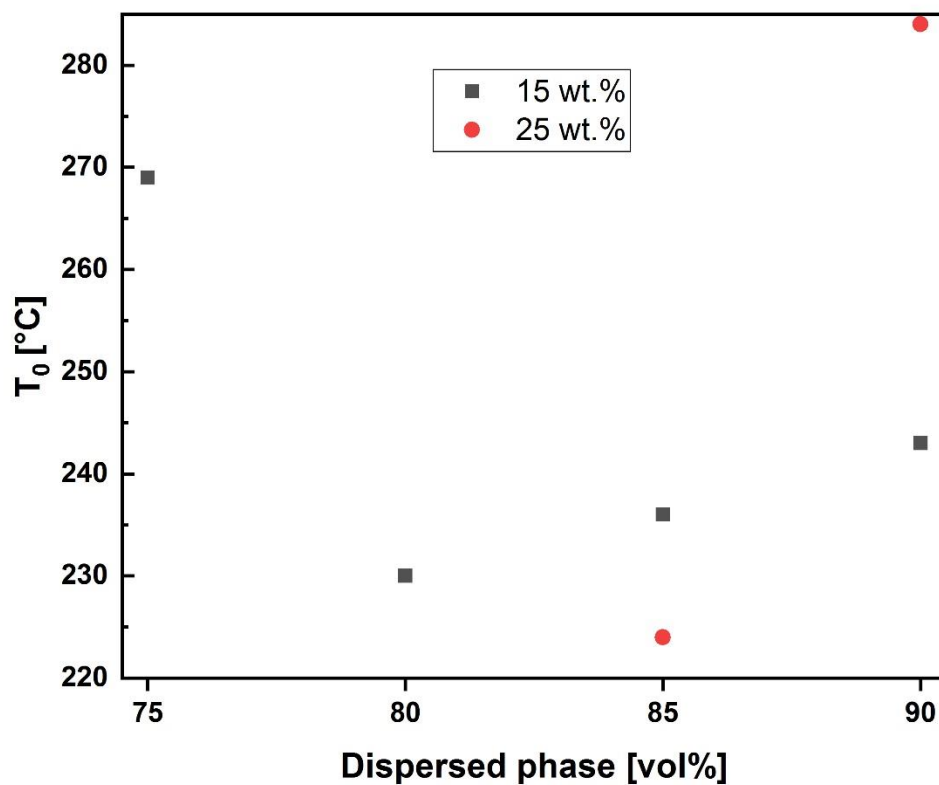


Figure 8 Dependence between extrapolated onset temperature  $T_0$ , internal phase ratio and surfactant content (7.5 wt.%, 15 wt.%, 25 wt.%)

In DSC measurements, below 0°C melting peaks of the surfactant Span® 80 were observed (Figure 9).

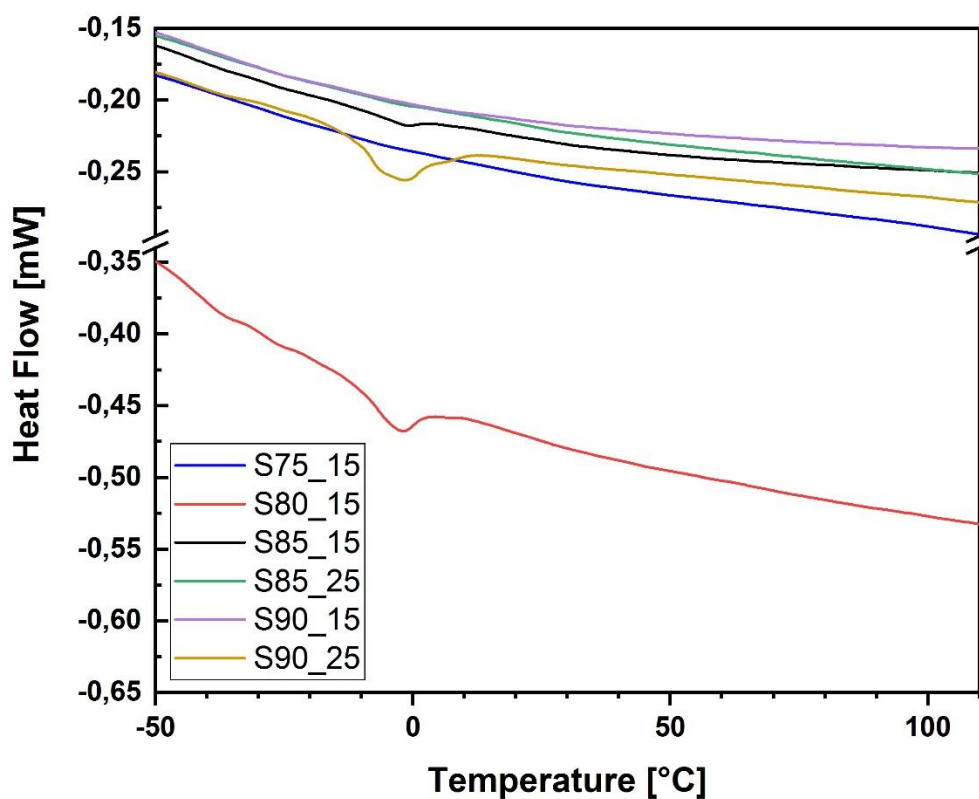


Figure 9 DSC thermograms from the second run

For the samples with internal phases of 85 vol% and 90 vol% the ionic conductivity decreased, when varying the surfactant ratio from 15 wt.% to 25 wt.% (Figure 10). A potential reason for this is the irregular microstructure. However, their standard deviations are nearly an order of magnitude higher in comparison to their counterparts with a surfactant amount of 15 wt.%, which indicates a higher inhomogeneity of the polyHIPE scaffolds for S85\_25 and S90\_25. The higher the porosities of the samples containing 15 wt.% surfactant (Figure 10), the greater was their ionic conductivity, which is consistent with literature<sup>20</sup>.

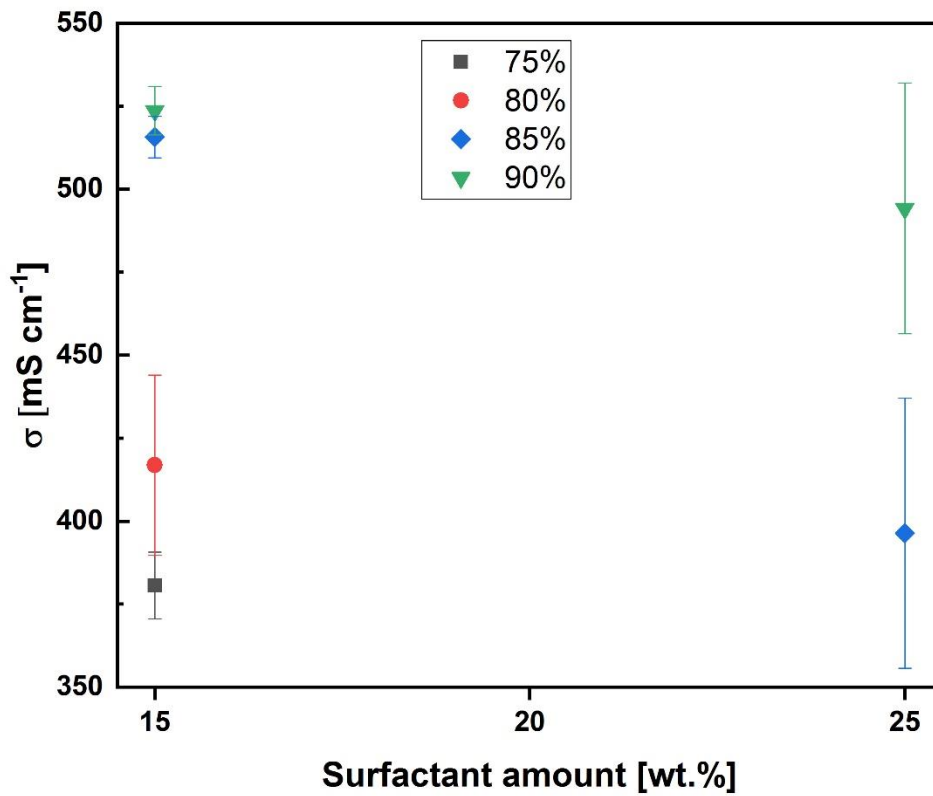


Figure 10 Relationship between surfactant ratio and conductivity measured at 25°C

Low MacMullin numbers and low tortuosities (Table 5) point to little hindrance of the ionic conductivity of the electrolyte through the separator matrix.

Table 5 Porosity, MacMullin Number: measured ionic conductivity for KOH was 1737.86 mS·cm<sup>-1</sup>, tortuosity

Sample	ε Porosity [-]	N <sub>M</sub> MacMullin Number [-]	τ Tortuosity [-]
S75_15	0.75	4.6±0.10	3.4±0.08
S80_15	0.82	4.2±0.21	3.4±0.18
S85_15	0.87	3.4±0.04	2.9±0.03
S85_25	0.87	4.4±0.36	3.8±0.31
S90_15	0.90	3.3±0.04	3.0±0.03
S90_25	0.90	3.5±0.19	3.2±0.17

In Figure 11 the first charge (black) and discharge (red) curve are depicted. During charging the battery, the voltage rose to 2.3 V. The battery discharged at around 2.1 V, which is the nominal voltage of a lead acid battery indicating, that charge and discharge processes take

place. Voltage rapidly drops to 1.76 V, when the battery is fully discharged. Only the first cycle is depicted, since the built battery cell is subjected to repeated charge and discharge cycles. Currently, the tests are still running.

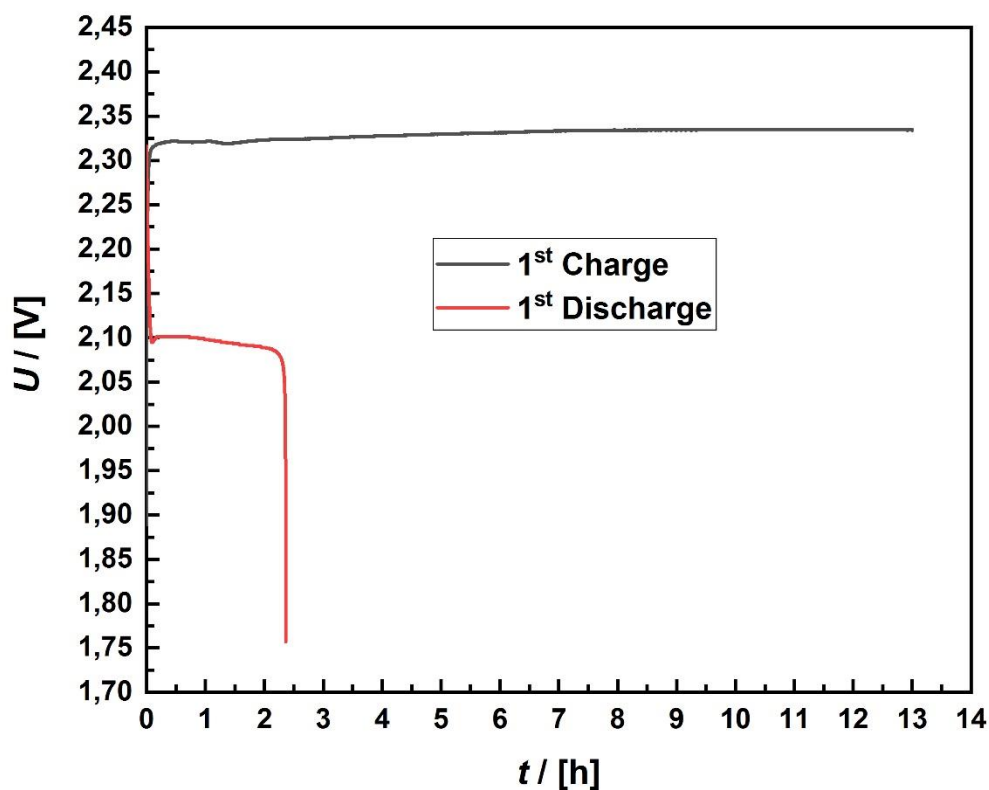


Figure 11 Charge and discharge curve of a lead acid battery (first cycle)

### 3.1. Results and discussion on non-aqueous polymerised high internal phase emulsions (polyHIPEs)

Already in 1970 Jasinski and Carroll<sup>45</sup> stated, that 1N LiClO<sub>4</sub> in PC reacts with most oxidisable materials at elevated temperatures. An application in commercial lithium cells is therefore not suitable. But because it is easy to handle and the experiments containing LiClO<sub>4</sub> could be carried out in air, it was used to find the highest possible lithium salt amount at which the formation of a polyHIPE could still be achieved (*Figure 12*) proves, that polyHIPEs with classical structure can be formed by using an internal phase containing 3.9M LiClO<sub>4</sub>. Average pore diameters are in the range of  $1.99 \pm 0.74 \mu\text{m}$  and the average pore throat sizes are  $0.70 \pm 0.22 \mu\text{m}$ .

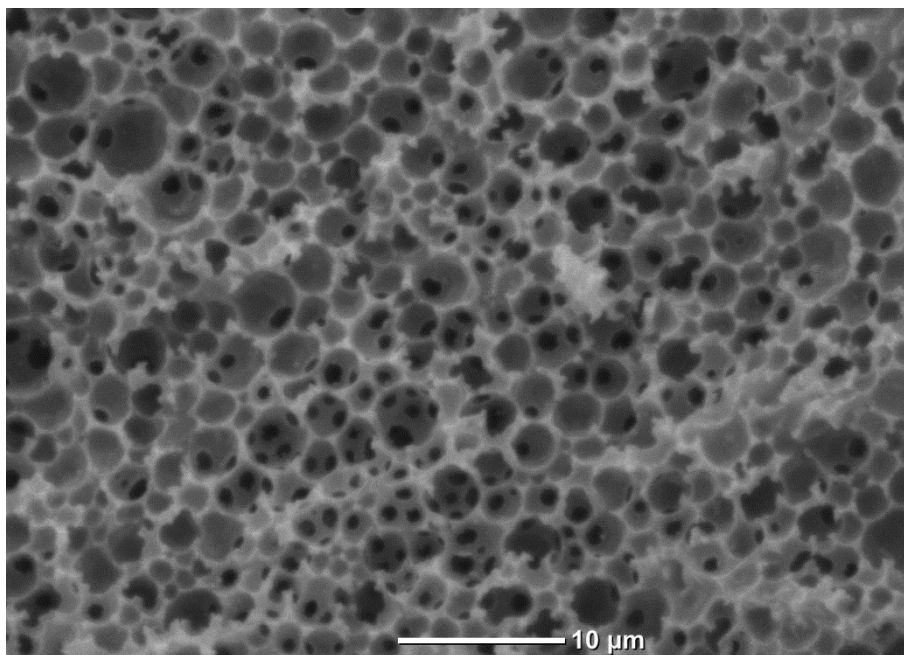


Figure 12 SEM image of a polyHIPE film with an internal phase of 85vol % with 3.9M  $\text{LiClO}_4$  dissolved in 50:50 EC/PC and a surfactant amount of 15 wt. %

PC is recognized as glass-forming liquid, which do not tend to crystallize<sup>46,47</sup>. Between  $-180^\circ\text{C}$  and  $120^\circ\text{C}$  a single glass transition (*Figure 13*) was observed for all tested lithium salts excluding  $\text{LiClO}_4$  (*Table 6*). In this temperature range - except of  $\text{LiClO}_4$  - all electrolytes can be used, since the data prove, the absence of melting peaks and therefore, the occurrence of crystallisation and the associated loss in ionic conductivity can be eliminated. Electrolytes, which are composed of the lithium salts  $\text{LiBF}_4$ ,  $\text{LiASF}_6$ ,  $\text{LiPF}_6$  and  $\text{LiTFSI}$  will not crystallize in the specified temperature range.

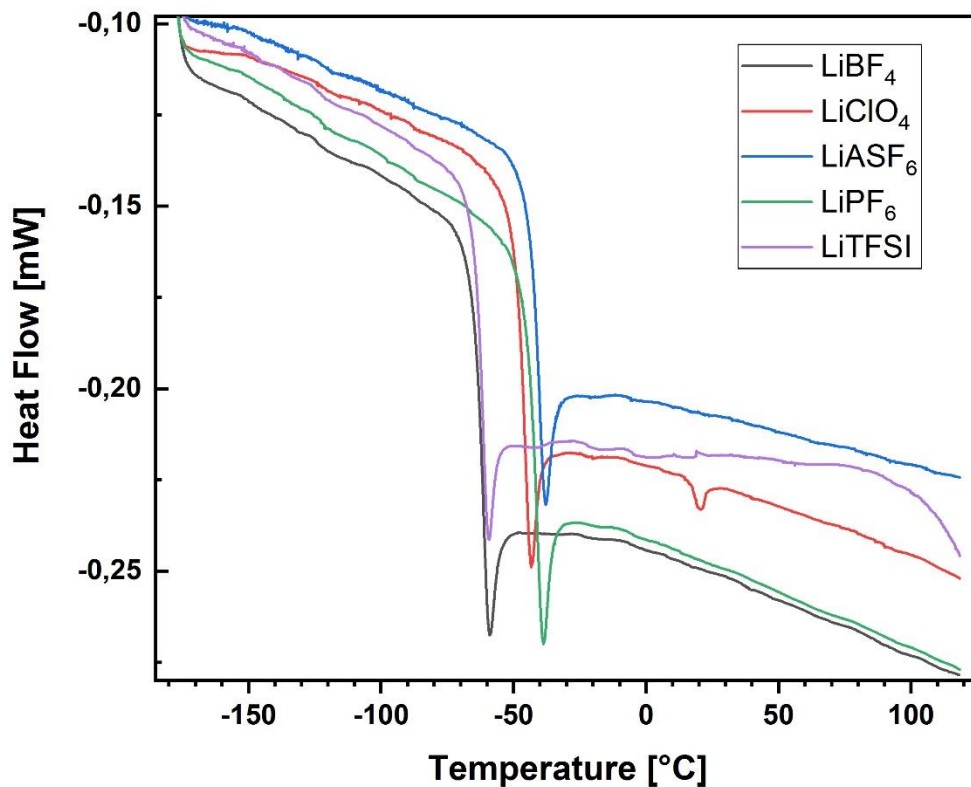


Figure 13 DSC curves (second run) of different 4.9M concentrated lithium salts in 50:50 EC/PC

Table 6 Glass transition ( $T_g$ ) and melting ( $T_m$ ) temperatures obtained from the DSC measurements (Figure 13)

sample	$T_g$ [°C]	$T_g$ [K]	$T_m$ [°C]	$T_m$ [K]
LiBF <sub>4</sub>	-63.17	209.98		
LiClO <sub>4</sub>	-47.97	225.18	16.86	290.01
LiAsF <sub>6</sub>	-42.97	230.7		
LiPF <sub>6</sub>	-43.62	229.53		
LiTFSI	-62.90	210.25		

Temperature dependencies of the ionic conductivity (Table 6) of different 4.9 M lithium salts are shown in the Arrhenius plots (Figure 14). By means of Vogel-Fulcher-Tamman equation:

$$\sigma = \frac{A}{\sqrt{T}} \exp\left(-\frac{E_a}{R} \frac{1}{T - T_0}\right) \quad (7)$$

The temperature can be linked to the ionic conductivity.  $A$  is a fitting parameter and is equal to the utmost electrical conductivity it would possess at infinite temperature.  $E_a$  is the activation energy for electrical conduction, which represents the necessary energy for an ion to leap to a free hole.  $T_0$  is the ideal glass transition temperature, where the fluidity is 0. Generally it is 10 to 20°C lower than the measured glass transition temperature<sup>48</sup>.  $R$  in equation (7) is the gas constant. High accuracy, shown by the  $R^2$  values (Table 7) verify the fitting of the Vogel-Fulcher-Tamman equation (7) to describe the temperature dependency of the electrical conductivity.

Table 7 VTF parameters obtained by applying equation (7) onto the measured ionic conductivities for different 4.9M concentrated lithium salts in 50:50 EC/PC

sample	$A T^{-1/2}$ [ $S \cdot cm^{-1} \cdot K^{1/2}$ ]	$E_a$ [ $kJ \cdot mol^{-1}$ ]	$T_0$ [K]	$R^2$
LiBF <sub>4</sub>	9.37	7.77	162.18	0.999
LiClO <sub>4</sub>	11.86	6.93	193.52	0.999
LiAsF <sub>6</sub>	23.65	7.59	194.31	0.999
LiPF <sub>6</sub>	16.71	6.97	198.06	0.999
LiTFSI	5.95	6.96	168.84	0.999

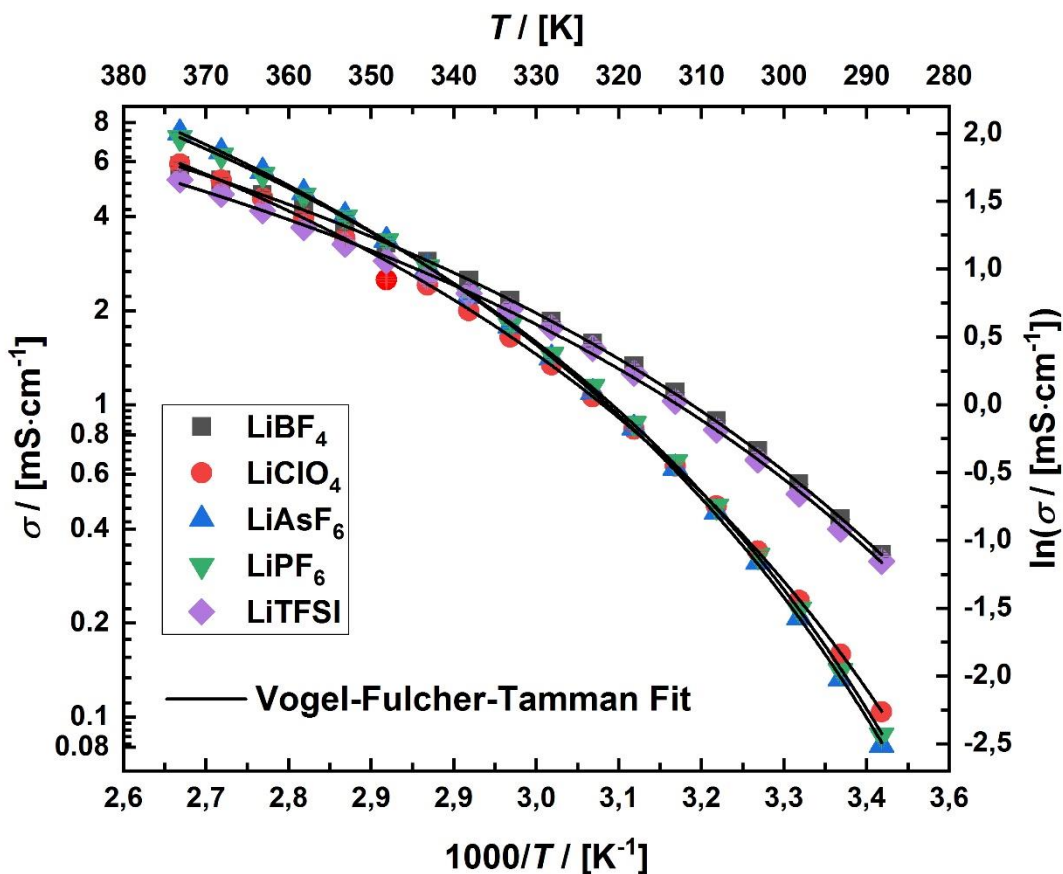


Figure 14 Arrhenius plots of the measured ionic conductivities ( $\sigma$ ) for the 4.9M lithium salts in 50:50 EC/PC. The solid lines represent the applied Vogel-Fulcher Tamman fit

Over a broad temperature range  $\text{LiBF}_4$  had the highest conductivity values (Figure 14). Subsequently, a polyHIPE with an internal phase of 4.9 M  $\text{LiBF}_4$  dissolved in 50:50 EC/PC ( $\text{LiBF}_4\text{_{Sep}}$ ) was prepared and its conductivity was measured at 25°C. To illustrate the significant influence of PC on the conductivity in the EC/PC electrolyte mixture, 4.9M  $\text{LiBF}_4$  were dissolved in pure EC (Figure 15c). Between 15°C and 100°C the conductivity values were much higher, when using a mix of EC/PC. Especially at higher temperatures PC's impact on ionic conductivity is clearly visible.

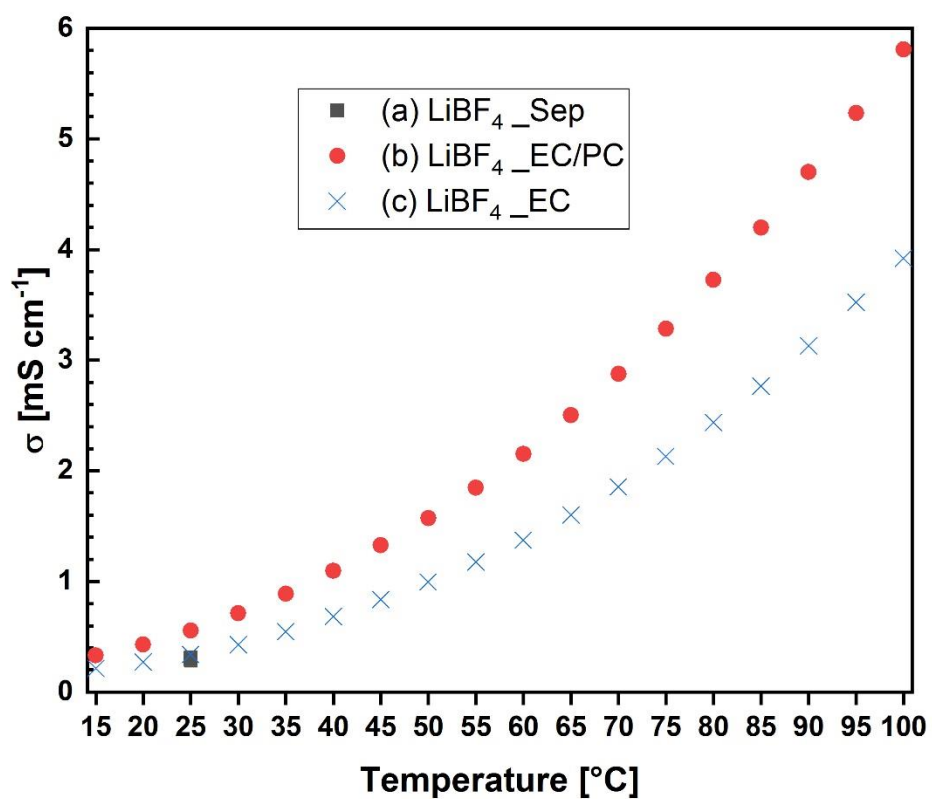


Figure 15 Conductivity of (a) a polyHIPE filled with 4.9M  $\text{LiBF}_4$  in 50:50 EC/PC, (b) 4.9M  $\text{LiBF}_4$  dissolved in 50:50 EC/PC, (c) 4.9M  $\text{LiBF}_4$  dissolved in EC

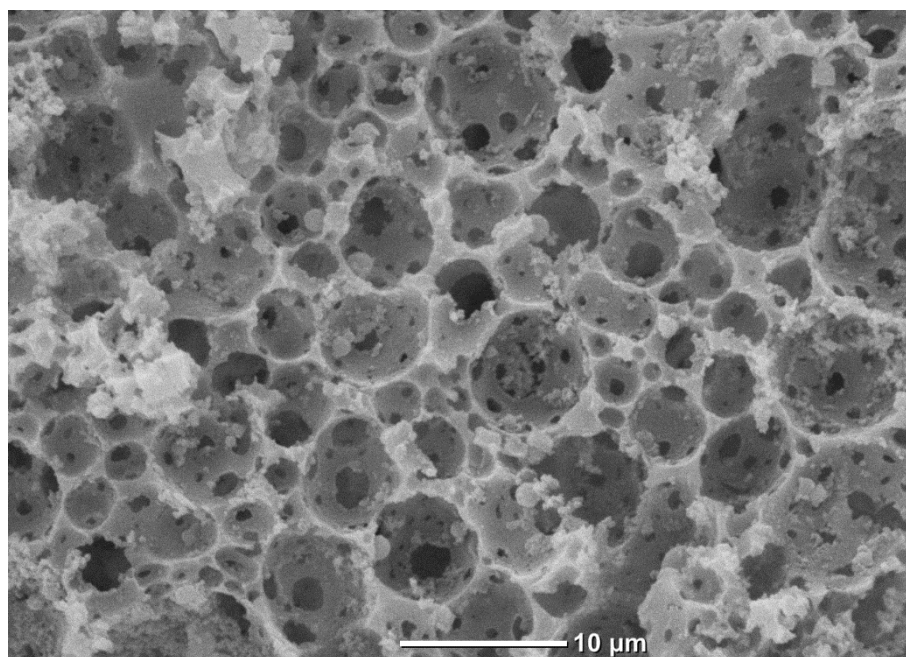


Figure 16 SEM image of a polyHIPE film with an internal phase of 85vol % with 4.9M  $\text{LiBF}_4$  dissolved in 50:50 EC/PC and a surfactant amount of 15 wt.%

The average pore diameter of the LiBF<sub>4</sub>\_Sep sample was 2.79±2.08 μm and the average pore throat size 0.52±0.4 μm. The high standard derivations for the average pore size and the average pore throat diameter suggested a very inhomogeneous polyHIPE. Though, a conductivity of 0.3 ±0.07 mS·cm<sup>-1</sup> and a low MacMullin number of 2 indicated, that it has little impact on the conductivity values. This points to much complex relation between conductivity and microstructure. Further investigations are needed. In comparison, commercial separators for lithium ion batteries have MacMullin numbers of 14 to 16. The lowest MacMullin number was reported for the commercially available lithium battery separator Celgard 2500 with a value of 4.5<sup>39</sup>, which is still more than twice as big as for LiBF<sub>4</sub>\_Sep.

The anode and cathode were isolated from each other by a 570 μm thick polyHIPE separator (*Figure 17*).

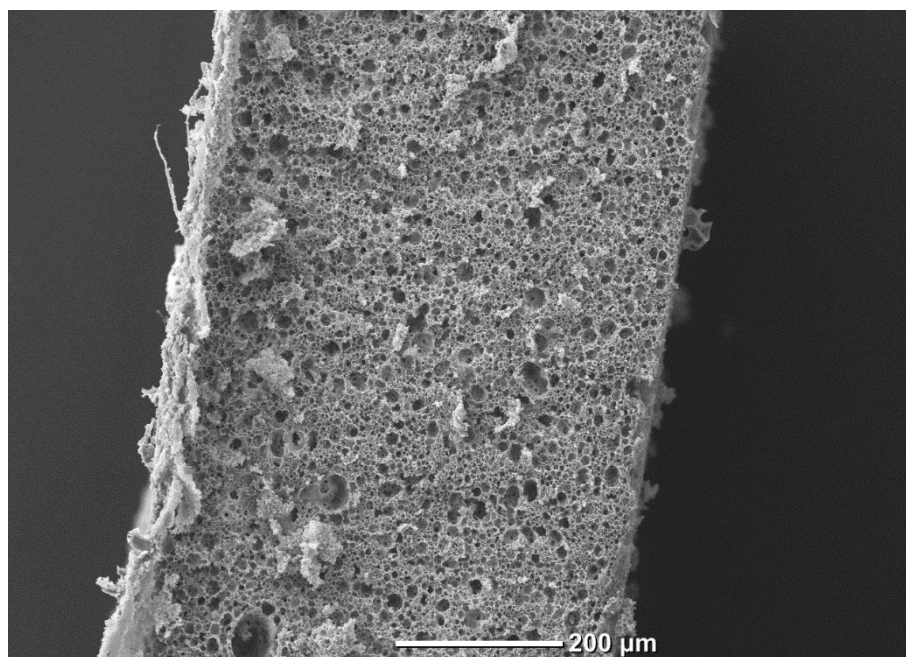


Figure 17 SEM picture: polyHIPE consisting of an internal phase of 4.9M LiBF<sub>4</sub> dissolved in 50:50 EC/PC

After 10 h the battery is fully discharged (*Figure 18*). With a capacity of 1.7 mAh for a 0.1 C-rate. Ideally 0.17 mA can be drawn for 10 hours before the battery is completely discharged. After less than 12 h it is fully charged again with a 0.08 C- rate. The battery should not be charged with more than 0.17 mA. Battery cycling tests are still running, therefore only the first cycle is shown in *Figure 18*.

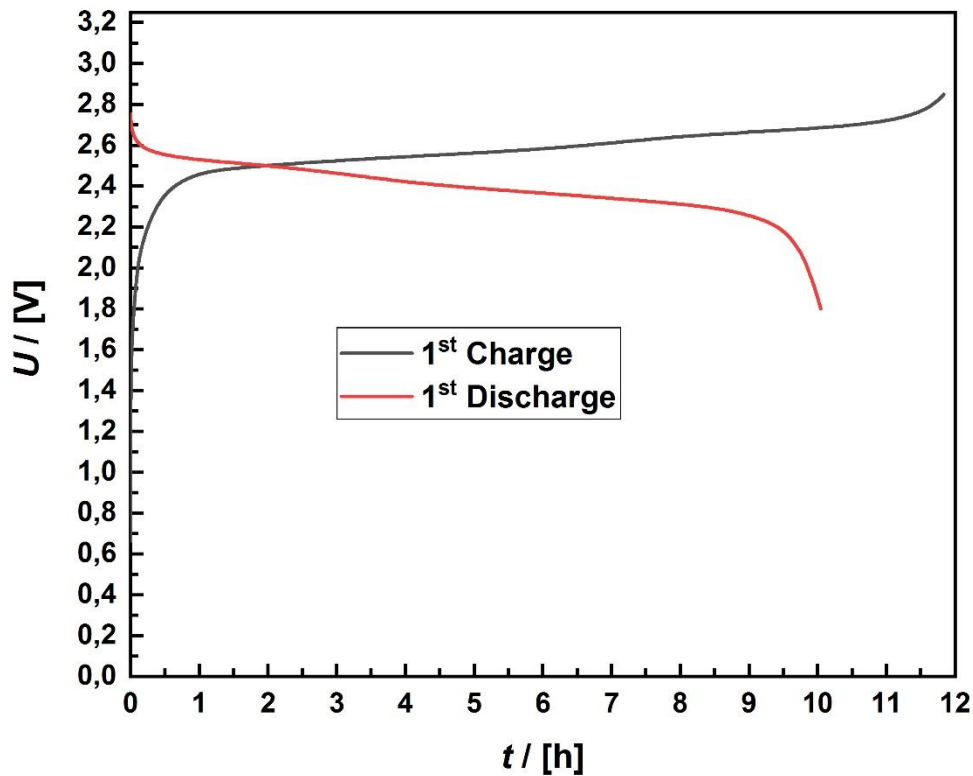


Figure 18 Charge and discharge curve of a lithium cell containing 4.9M LiBF<sub>4</sub> and 50:50 EC/PC as electrolyte (first cycle)

Table 8 Summarized charge and discharge values of different investigated cell types

sample	$I_{\text{charge}}$ [mA]	$I_{\text{discharge}}$ [mA]	$U_{\text{upper}}$ [V]	$U_{\text{lower}}$ [V]	Efficiency 1 <sup>st</sup> Cycle
Li-Ion	0.17	0.17	2.85	1.8	0.89
Lead-Acid	1.25	0.625	2.47	1.75	0.09
NiMH	10	10	1.42	1	0.75

Table 8 shows charge and discharge values of the different investigated batteries. The low efficiency for the lead-acid system in the 1<sup>st</sup> cycle (Table 8) can be attributed to the cell construction and incomplete use of the active material. To achieve a suitable cell construction, the positive- and negative electrode should be porous and able to absorb the electrolyte, to provide the greatest possible interface area for the electrochemical reaction. To ensure safe power-supplying reactions and current diversion, an electrode framework made of antimonial lead, would be necessary. In our cell assembly, merely two lead foils were used, representing the electrodes. Their efficiency is little (Table 8), since the power-supplying reactions were too

---

slow and the voltage collapses already at minimum current load. Active materials take part in the electrochemical charge and discharge reactions. These include the negative-, the positive electrode and the electrolyte. The discharge of the negative- and positive material stops before the whole charged active material is transformed in discharged active material, due to the fact, that pure lead sulphate ( $\text{PbSO}_4$ ) is non-conductive. In lead acid batteries and other galvanic cells, only 50% of the supplied active materials can be used. Moreover, to start the charging process again, active materials - produced during the charging step – are needed, therefore a fully discharge is not possible.<sup>50</sup>

## 4. Conclusion

This thesis showed the possibility to manufacture in situ filled separators with the desired electrolyte via a one-pot synthesis. In comparison much more steps and time are needed to produce separators and fill them with the electrolyte for commercial NiMH<sup>8-</sup>, lead acid<sup>22-</sup>, and lithium<sup>51</sup> systems. Furthermore, the polyHIPE scaffold is chemically stable over a broad range of electrolytes. Water-based electrolytes -5M  $\text{H}_2\text{SO}_4$  and 20% KOH - were used in a pH spectrum of 1 to 14 and in both environments the separator matrix was stable. Furthermore, it was chemically inert in superconcentrated electrolytes, applied in lithium batteries. All formulations were processed by printing the liquid HIPE formulations. Systems containing KOH or  $\text{H}_2\text{SO}_4$  as internal phase were all processed in air and indicates operational simplicity during manufacturing. An open porous microstructure was achieved by reaching porosities up to 90%, while ensuring the classical polyHIPE structure. For the water-based electrolytes, used in polyHIPEs as dispersed phase, average pore size of lower than 2  $\mu\text{m}$  were reached. Thermal stabilities of at least 200°C were observed, implying no significant failure of the separator scaffold should occur during battery cycling.

---

## 5. References

1. Arora, P. & Zhang, Z. Battery separators. *Chem. Rev.* **104**, 4419–4462 (2004).
2. Daniel, C. & Besenhard, J. O. *Handbook of Battery Materials: Second Edition*. *Handbook of Battery Materials: Second Edition* (2011). doi:10.1002/9783527637188
3. Shirshova, N. *et al.* Polymerised high internal phase ionic liquid-in-oil emulsions as potential separators for lithium ion batteries. *J. Mater. Chem. A* **1**, 9612 (2013).
4. Shirshova, N., Bismarck, A. & Steinke, J. H. G. Ionic liquids as internal phase for non-aqueous polyHIPEs. *Macromol. Rapid Commun.* **32**, 1899–1904 (2011).
5. Kot, E., Shirshova, N., Bismarck, A. & Steinke, J. H. G. Non-aqueous high internal phase emulsion templates for synthesis of macroporous polymers in situ filled with cyclic carbonate electrolytes. *RSC Adv.* **4**, 11512–11519 (2014).
6. Yamada, Y. & Yamada, A. Review—Superconcentrated Electrolytes for Lithium Batteries. *J. Electrochem. Soc.* **162**, A2406–A2423 (2015).
7. Kritzer, P. Separators for nickel metal hydride and nickel cadmium batteries designed to reduce self-discharge rates. *Journal of Power Sources* **137**, 317–321 (2004).
8. Kritzer, P. & Cook, J. A. Nonwovens as Separators for Alkaline Batteries. *J. Electrochem. Soc.* **154**, A481 (2007).
9. Ikoma, M., Hoshina, Y., Matsumoto, I. & Iwakura, C. Self-discharge mechanism of sealed-type nickel/metal-hydride battery. *J. Electrochem. Soc.* **143**, 1904–1907 (1996).
10. Leblanc, P., Blanchard, P. & Senyarich, S. Self-discharge of sealed nickel-metal hydride batteries: Mechanisms and improvements. *J. Electrochem. Soc.* **145**, 844–847 (1998).
11. Nagarajan, G. S. & Van Zee, J. W. Characterization of the performance of commercial Ni/MH batteries. *J. Power Sources* **70**, 173–180 (1998).
12. Bennett, J. & Ming Choi, W. Overview of the effect of separator on the performance of the nickel metal hydride battery. *IEEE* 153–157 (1998).
13. Jiao, X., Cheng, B., Kang, W. & Yang, W. Nickel-metal hydride battery separators fabricated from sulfonated nonwovens. *J. Appl. Polym. Sci.* **109**, 272–275 (2008).
14. Li, X., Song, Y., Wang, L., Xia, T. & Li, S. Self-discharge mechanism of Ni-MH battery by using acrylic acid grafted polypropylene separator. *Int. J. Hydrogen Energy* **35**, 3798–3801 (2010).
15. Tian, Y., Gao, H., Wang, J., Jin, X. & Wang, H. Preparation of hydroentangled CMC composite nonwoven fabrics as high performance separator for nickel metal hydride battery. *Electrochim. Acta* **177**, 321–326 (2015).
16. Chang, S., Young, K.-H. & Lien, Y.-L. Reviews of European Patents on Nickel/Metal Hydride Batteries. *Batteries* **3**, 25 (2017).
17. Young, K., Cai, X. & Chang, S. Reviews on Chinese Patents Regarding the Nickel/Metal Hydride Battery. *Batteries* **3**, 24 (2017).

18. Yan, S., Young, K.-H. & Ng, K. Y. Effects of Salt Additives to the KOH Electrolyte Used in Ni/MH Batteries. *Batteries* **1**, 54–73 (2015).
19. Gilliam, R. J., Graydon, J. W., Kirk, D. W. & Thorpe, S. J. A review of specific conductivities of potassium hydroxide solutions for various concentrations and temperatures. *Int. J. Hydrogen Energy* **32**, 359–364 (2007).
20. Böhnstedt, W. Automotive lead/acid battery separators: a global overview. *J. Power Sources* **59**, 45–50 (1996).
21. Wada, T. & Hirashima, T. Progress in polyethylene separators for lead-acid batteries. in *Journal of Power Sources* **107**, 201–210 (2002).
22. Böhnstedt, W. Separators. *Handb. Batter. Mater.* 245–292 (1999). doi:10.1002/9783527637188.ch11
23. Cameron, N. R. & Sherrington, D. C. High Internal Phase Emulsions (HIPEs) - Structure, Properties and Use in Polymer Preparation. in *Advances in Polymer Science* **126**, 163–214 (1996).
24. Lissant, K. J. The geometry of high-internal-phase-ratio emulsions. *J. Colloid Interface Sci.* **22**, 462–468 (1966).
25. Silverstein, M. S. PolyHIPEs: Recent advances in emulsion-templated porous polymers. *Progress in Polymer Science* **39**, 199–234 (2014).
26. Xu, K. Nonaqueous liquid electrolytes for lithium-based rechargeable batteries. *Chem. Rev.* **104**, 4303–4417 (2004).
27. Zhao, H. *et al.* Propylene Carbonate (PC)-Based Electrolytes with High Coulombic Efficiency for Lithium-Ion Batteries. *J. Electrochem. Soc.* **161**, A194–A200 (2013).
28. Pistoia, G., Rossi, M. De & Scrosati, B. Study of the Behavior of Ethylene Carbonate as a Nonaqueous Battery Solvent. *J. Electrochem. Soc.* **117**, 500 (1970).
29. Pistoia, G. Nonaqueous Batteries with LiClO<sub>4</sub>-Ethylene Carbonate as Electrolyte. *J. Electrochem. Soc.* **118**, 153–158 (1971).
30. Abraham, K. M. ; & Alamgir, M. Li<sup>+</sup>-Conductive Solid Polymer Electrolytes with Liquid-Like Conductivity. *J. Electrochem. Soc.* **137**, 1657–1658 (1990).
31. Fong, Rosamaría; von Sacken, Ulrich; Dahn, J. R. Studies of Lithium Intercalation into Carbons Using Nonaqueous Electrochemical Cells. *J. Electrochem. Soc.* **137**, 2009 (1990).
32. Chen, H. P., Fergus, J. W. & Jang, B. Z. The Effect of Ethylene Carbonate and Salt Concentration on the Conductivity of Propylene Carbonate|Lithium Perchlorate Electrolytes. *J. Electrochem. Soc.* **147**, 399–406 (2000).
33. Chu, P. P. & He, Z. P. Lithium complex in polyacrylonitrile/EC/PC gel-type electrolyte. *Polymer (Guildf)*. **42**, 4743–4749 (2001).
34. Peled, E. The Electrochemical Behavior of Alkali and Alkaline Earth Metals in Nonaqueous Battery Systems—The Solid Electrolyte Interphase Model. *J. Electrochem. Soc.* **126**, 2047 (1979).

- 
35. Zheng, J., Lochala, J. A., Kwok, A., Deng, Z. D. & Xiao, J. Research Progress towards Understanding the Unique Interfaces between Concentrated Electrolytes and Electrodes for Energy Storage Applications. *Advanced Science* **4**, (2017).
  36. Jeong, S.-K., Inaba, M., Iriyama, Y., Abe, T. & Ogumi, Z. Electrochemical Intercalation of Lithium Ion within Graphite from Propylene Carbonate Solutions. *Electrochem. Solid-State Lett.* **6**, A13 (2003).
  37. Jeong, S. K., Inaba, M., Iriyama, Y., Abe, T. & Ogumi, Z. Interfacial reactions between graphite electrodes and propylene carbonate-based solutions: Electrolyte-concentration dependence of electrochemical lithium intercalation reaction. *J. Power Sources* **175**, 540–546 (2008).
  38. MacMullin, R. B. & Muccini, G. A. Characteristics of porous beds and structures. *AIChE J.* **2**, 393–403 (1956).
  39. Landesfeind, J., Hattendorff, J., Ehrl, A., Wall, W. A. & Gasteiger, H. A. Tortuosity Determination of Battery Electrodes and Separators by Impedance Spectroscopy. *J. Electrochem. Soc.* **163**, A1373–A1387 (2016).
  40. Livshin, S. & Silverstein, M. S. Crystallinity and cross-linking in porous polymers synthesized from long side chain monomers through emulsion templating. *Macromolecules* **41**, 3930–3938 (2008).
  41. Williams, J. M. & Wroblewski, D. A. Spatial distribution of the phases in water-in-oil emulsions. open and closed microcellular foams from cross-linked polystyrene. *Langmuir* **4**, 656–662 (1988).
  42. Cameron, N. R. High internal phase emulsion templating as a route to well-defined porous polymers. *Polymer* **46**, 1439–1449 (2005).
  43. P. Arora; S. Frisk; L. Zhang. Batteries including improved fine fiber separators. (2006).
  44. Panasonic. *Individual data sheet: NICKEL METAL HYDRIDE HANDBOOK AUGUST 2005*. (2005).
  45. Jasinski, R. & Carroll, S. Thermal Stability of a Propylene Carbonate Electrolyte. *J. Electrochem. Soc.* **117**, 218 (1970).
  46. Stallworth, P. . *et al.* NMR, DSC and high pressure electrical conductivity studies of liquid and hybrid electrolytes. *J. Power Sources* **81–82**, 739–747 (1999).
  47. Fontanella, J. J., Wintersgill, M. C. & Immel, J. J. Dynamics in propylene carbonate and propylene carbonate containing LiPF<sub>6</sub>. *J. Chem. Phys.* **110**, 5392–5402 (1999).
  48. Angell, C. A. & Sare, E. J. Glass-forming composition regions and glass transition temperatures for aqueous electrolyte solutions. *J. Chem. Phys.* **52**, 1058–1068 (1970).
  49. Hayamizu, K., Aihara, Y., Nakagawa, H., Nukuda, T. & Price, W. S. Ionic conduction and ion diffusion in binary room-temperature ionic liquids composed of [emim][BF<sub>4</sub>] and LiBF<sub>4</sub>. *J. Phys. Chem. B* **108**, 19527–19532 (2004).
  50. Hamann, C.H.; Vielstich, W. *Elektrochemie*. (Wiley-VCH Verlag GmbH, Weinheim, 2005).
  51. Lee, H., Yanilmaz, M., Toprakci, O., Fu, K. & Zhang, X. A review of recent developments

in membrane separators for rechargeable lithium-ion batteries. *Energy Environ. Sci.* **7**, 3857–3886 (2014).

---



---

## List of Figures

Figure 1 SEM images of polyHIPE films: (a) K75_7.5, (b) K75_15, (c) K75_25, (d) K80_7.5, (e) K80_15, (f) K80_25, (g) K85_7.5, (h) K85_15, (i) K85_25, (j) K90_7.5, (k) K90_15, (l) K90_25, (m) K95_15. For composition see Table 1.....	15
Figure 2 Dependence between extrapolated onset temperature $T_0$ , internal phase ratio and surfactant content (7.5 wt.%, 15 wt.%, 25 wt.%) .....	18
Figure 3 Representative DSC thermograms from the second run for the scaffolds with 75 vol% of internal phase and their respective surfactant ratio (7.5 wt. %, 15 wt.%, 25 wt.%) .....	19
Figure 4 Relationship between surfactant ratio and conductivity measured at 25°C.....	20
Figure 5 Charge and discharge curve of a NiMH battery (first cycle) .....	23
Figure 6 Charging and discharging over 31 cycles (NiMH system) .....	24
Figure 7 SEM images of polyHIPE films: (a) S75_15, (b) S80_15, (c) S85_15, (d) S85_25, (e) S90_15, (f) S90_25. For sample composition see Table 1. ....	25
Figure 8 Dependence between extrapolated onset temperature $T_0$ , internal phase ratio and surfactant content (7.5 wt.%, 15 wt.%, 25 wt.%) .....	27
Figure 9 DSC thermograms from the second run .....	28
Figure 10 Relationship between surfactant ratio and conductivity measured at 25°C.....	29
Figure 11 Charge and discharge curve of a lead acid battery (first cycle) .....	30
Figure 12 SEM image of a polyHIPE film with an internal phase of 85vol % with 3.9M $\text{LiClO}_4$ dissolved in 50:50 EC/PC and a surfactant amount of 15 wt.%.....	31
Figure 13 DSC curves (second run) of different 4.9M concentrated lithium salts in 50:50 EC/PC .....	32
Figure 14 Arrhenius plots of the measured ionic conductivities ( $\sigma$ ) for the 4.9M lithium salts in 50:50 EC/PC. The solid lines represent the applied Vogel-Fulcher Tamman fit .....	34
Figure 15 Conductivity of (a) a polyHIPE filled with 4.9M $\text{LiBF}_4$ in 50:50 EC/PC, (b) 4.9M $\text{LiBF}_4$ dissolved in 50:50 EC/PC, (c) 4.9M $\text{LiBF}_4$ dissolved in EC.....	35

---

---

Figure 16 SEM image of a polyHIPE film with an internal phase of 85vol % with 4.9M LiBF <sub>4</sub> dissolved in 50:50 EC/PC and a surfactant amount of 15 wt.%.....	35
Figure 17 SEM picture: polyHIPE consisting of an internal phase of 4.9M LiBF <sub>4</sub> dissolved in 50:50 EC/PC.....	36
Figure 18 Charge and discharge curve of a lithium cell containing 4.9M LiBF <sub>4</sub> and 50:50 EC/PC as electrolyte (first cycle) .....	37

---

---

## List of Tables

Table 1 Sample composition of aqueous polyHIPEs used KOH as internal phase (abbreviated K) and H <sub>2</sub> SO <sub>4</sub> as internal phase (abbreviated S). Used materials for the preparation of aqueous polyHIPEs are listed in chapter 2.1.1 for KOH as dispersed phase and 2.1.2 for H <sub>2</sub> SO <sub>4</sub> as dispersed phase.....	7
Table 2 Properties of polyHIPEs prepared with KOH as internal phase: specific surface area, average pore diameter <D>, average pore throat diameter <d>, skeletal density, porosity, onset temperature T <sub>0</sub> .....	16
Table 3 Porosity, MacMullin Number: measured ionic conductivity for KOH was 484.42 mS cm <sup>-1</sup> , tortuosity.....	22
Table 4 Properties of polyHIPEs prepared with H <sub>2</sub> SO <sub>4</sub> as internal phase: specific surface area, average pore diameter <D>, average pore throat diameter <d>, skeletal density, porosity, onset temperature T <sub>0</sub> .....	26
Table 5 Porosity, MacMullin Number: measured ionic conductivity for KOH was 1737.86 mS·cm <sup>-1</sup> , tortuosity.....	29
Table 6 Glass transition (T <sub>g</sub> ) and melting (T <sub>m</sub> ) temperatures obtained from the DSC measurements (Figure 13) .....	32
Table 7 VTF parameters obtained by applying equation (7) onto the measured ionic conductivities for different 4.9M concentrated lithium salts in 50:50 EC/PC .....	33
Table 8 Summarized charge and discharge values of different investigated cell types .....	37

## Kurzfassung

Separatoren nehmen eine Schlüsselfunktion in allen Batterien ein. Zum einen müssen sie den Durchgang der Ladungsträger ermöglichen, andererseits die Funktion einer Barriere einnehmen, um die Anode und Kathode räumlich voneinander zu isolieren. Um diese gegensätzlichen Aufgaben zu erfüllen, ist der Einsatz eines porösen Materials essentiell. Die Herstellung von kommerziell erhältlichen Separatoren – ganz gleich für welches Batteriesystem sie produziert werden - ist sehr zeitaufwendig, da sie multiple Verfahrensschritte beinhalten. PolyHIPEs stellen das ideale Material dar: Sie ermöglichen eine Eintopfreaktion, in der der Elektrolyt in-situ hinzugegeben werden wird und aufgrund ihrer hochporösen Struktur erreichen sie Porositäten von 75-94%. Ihre Anwendung ist nicht durch den pH-Wert des Elektrolyten beschränkt, da die polyHIPE Separatoren in saurer Umgebung sowie in basischer Umgebung stabil sind. Durch das Emulsion Templating wird noch vor der Polymerisation eine direkte Bedruckung der Elektroden ermöglicht. Separatoren reduzieren die Leistung des Elektrolyten - und somit die der gesamten Batterie - durch ihre Matrix. Dies wird durch den MacMullin Kennwert ausgedrückt. Bei einem Idealwert von eins (keine Hinderung des Systems durch den Separator), erreichen die in dieser Arbeit getesteten Systeme Werte von zwei bis drei.